# Motor Cortical Representation of Speed and Direction During Reaching

DANIEL W. MORAN AND ANDREW B. SCHWARTZ
*The Neurosciences Institute, San Diego, California 92121*

**Moran, Daniel W. and Andrew B. Schwartz.** Motor cortical representation of speed and direction during reaching. *J. Neurophysiol.* 82: 2676–2692, 1999. The motor cortical substrate associated with reaching was studied as monkeys moved their hands from a central position to one of eight targets spaced around a circle. Single-cell activity patterns were recorded in the proximal arm area of motor cortex during the task. In addition to the well-studied average directional selectivity ("preferred direction") of single-cell activity, we also found the time-varying speed of movement to be represented in the cortical activity. A single equation relating motor cortical discharge rate to these two parameters was developed. This equation, which has both independent (speed only) and interactive (speed and direction) components, described a large portion of the time-varying motor cortical activity during the task. Electromyographic activity from a number of upper arm muscles was recorded during this task. Muscle activity was also found to be directionally tuned; however, the distributions of preferred directions were found to be significantly different from cortical activity. In addition, the effect of speed on cortical and muscle activity was also found to be significantly different.

## INTRODUCTION

How movement is represented in the brain is a central problem in motor physiology. Jackson (1875), based on his observations of epileptic seizures, helped establish the idea of an anatomic correlate for movement. Although Jackson himself did not believe in a discrete somatotopic representation in the cortex, others (Fritsch and Hitzig 1870; Leyton and Sherrington 1917; Schafer 1900), using electrical stimuli applied to the cerebrum to elicit muscle contraction, developed the idea that different locations in the motor cortex were responsible for movement of specific body parts. To date, this issue is still controversial, which may in part be due to static descriptions of movement-related activity. In the present set of studies, we examined the dynamic time-varying correlations between cortical activity and arm movement by developing a model of single-cell activity.

As the distributed nature of motor representations is becoming more clear (Kalaska and Crammond 1992), it has been shown that multiple parameters can be contained in the activity of single cells, that the same movement parameter can be found in multiple areas and that representations within a structure are labile (Alexander and Crutcher 1990a,b; Ashe and Georgopoulos 1994; Crutcher and Alexander 1990; Fritsch and Hitzig 1870; Fu et al. 1993, 1995; Sanes et al. 1990, 1992). With this in mind, we studied neuronal activity in two distinct cortical areas during three different tasks while examining the representation of two movement parameters as they were encoded throughout the duration of each task. This paper is the first of three in which we examine the dynamic activity of motor cortical cells during movement. Because movement can be characterized with velocity vectors that in turn are described by direction and magnitude (speed), we designed three types of experiments to examine these parameters. In the first study, described here, direction is constant and speed varied in each movement. In the second set of experiments, speed changed monotonically, and direction changed harmonically during spiral drawing. In the last paper, both parameters varied harmonically as monkeys drew figure-eights.

One of the most clearly represented parameters correlated with motor cortical activity is that of movement direction. Georgopoulos and colleagues (Georgopoulos et al. 1982; Schwartz et al. 1988) have used a center→out task in which subjects made arm movements from a central location to eight targets separated by equal angles. Single-cell activity, characterized by a rate averaged over the reaction (RT) and movement time (MT) to each target, varied in a regular way with direction. The rates, when plotted against movement direction, can be fit with a cosine function. Each cell has a peak discharge rate in a different "preferred direction," yet the tuning function spans all directions, showing that each cell's activity is modulated with all movements.

In the original observation of cosine directional tuning of motor cortical activity, a single average (calculated over the reaction and movement time of the task) discharge rate was compared with the angle of the peripheral target from the center (Georgopoulos et al. 1982). Using the average rate in the comparison to direction was valid because these point-to-point movements were fairly straight. Although direction is almost constant during an individual movement, the speed of the arm is not. Typically, point-to-point movements are made with bell-shaped velocity profiles (Georgopoulos et al. 1981; Morasso 1981; Soechting 1984). This is true of the center→out task; profiles to each target were bell-shaped and almost identical. Three experimental conditions (movements encompassing all directions, constant directions within each movement, and similar speed profiles across different movements) made it possible to remove the directional component from the recorded activity pattern while preserving the time-varying nondirectional component. We used these characteristics to construct an equation relating single-cell discharge rate to movement direction and speed.

The ensemble activity of motor cortical cells has been combined using the population vector algorithm (Georgopoulos et

The costs of publication of this article were defrayed in part by the payment of page charges. The article must therefore be hereby marked "*advertisement*" in accordance with 18 U.S.C. Section 1734 solely to indicate this fact.

 

al. 1983, 1988). These population vectors encode both instantaneous speed and direction within a movement (Schwartz 1993, 1994a). Although it is clear that the directional contributions of individual cells can sum to generate a population vector that points in the movement direction, the way these contributions combine so that the resultant vector magnitude reflects speed is more elusive. This was one of the issues we were able to address with our model of single-cell activity.

Motor cortical activity is considered to play an important role in regulating skeletal muscle contraction because a component of corticospinal fibers from this region project directly to motoneuronal pools and electrical currents applied to the precentral gyrus cause muscle contraction (Asanuma and Rosen 1972; Fritsch and Hitzig 1870; Landgren et al. 1962; Lemon et al. 1987; Woolsey 1958). Many reports have found motor cortical activity to be related to the force generated against imposed loads during behavioral experiments, suggesting again that motor cortical activity was facilitating muscle contraction (Dettmers et al. 1996; Evarts 1968; Georgopoulos et al. 1992; Humphrey et al. 1970; Kalaska et al. 1989; Maier et al. 1993; Schmidt et al. 1975; Thach 1978). Correlation techniques have shown that motor cortical activity can facilitate electromyographic (EMG) activity (Fetz and Cheney 1978; Fetz and Finnochio 1975; Mantel and Lemon 1987). To compare the features of this cortical activity to muscle activity patterns, we recorded EMG activity of the proximal arm muscles and subjected this activity to the same analyses that were applied to the single-cell activity patterns. Although cortical cell and muscle activity shared common features with respect to direction and speed, there were also clear differences showing that muscle activity was not simply related to firing patterns of individual motor cortical cells.

Most of the previous studies examining the relation between speed and motor cortical discharge rates have been in paradigms based on isolated elbow or wrist displacements with passive (Flament and Hore 1988; Lucier et al. 1975) or active (Bauswein et al. 1991; Burbaud et al. 1991; Butler et al. 1992; Hamada 1981) movement. These studies, which were designed to examine putative muscle spindle contributions to motor cortical activity, typically found a subpopulation of cells where mean firing rate was related to average angular velocity with a single movement direction. However, motor cortical activity was interpreted as not contributing to the generation of rapid single joint or oscillatory movement because cortical cells tended to be modulated in such a way that they lagged EMG (Butler et al. 1992) or fired after the movement began (Hamada 1981). In the present study with two-dimensional multijoint movements, we show that cell activity is modulated with speed in a way that depends on the cell's preferred direction, a parameter that cannot be determined in a single-joint task. Furthermore, in the present reaching task, the cortical activity pattern clearly precedes each increment of the movement in a continuous way throughout the task.

## METHODS

The behavioral paradigm, surgical procedures and general animal care were approved by the Institutional Animal Care and Use Committee. The outlines put forth by the Association for Assessment and Accreditation of Laboratory Animal Care and the Society for Neuroscience were followed.

### *Behavioral task*

Rhesus monkeys (*Maccaca mullata*) were trained using operant conditioning to perform point-to-point movements and draw various figures with a single finger. All movements were performed by the animal moving its finger along the planar surface of a vertically oriented glass touchscreen covering a computer graphics monitor. The surface of the touchscreen was lubricated daily with mineral oil to minimize finger friction. The finger position was digitized at 50 Hz with a resolution of 22 $\mu$m horizontally and 17.5 $\mu$m vertically. A sequence of tasks was performed after each cell was isolated.

The first task performed (the results of which are the subject of this paper) was a center→out task. The finger was moved from a center position to one of eight peripherally arranged targets equally spaced about a circle with a radius of 6.0 cm. Initially, a start target in the form of a circle with a radius of 1.0 cm appeared at the center of the touchscreen. As soon as the monkey placed its finger in the target, spike occurrence times began to be logged. After a brief hold time (hold-A) of 280–780 ms, the start circle disappeared as one of the eight target circles appeared. *X-Y* coordinates of the finger were measured from the touchscreen and recorded at this point. The animal was given 300 ms to move its finger from the center to the peripheral target while maintaining contact with the touchscreen. As soon as the monkey's finger crossed the outer border of the target circle, the sampling of movement data ceased. Spike data, however, were recorded until a second hold time (hold-B) of 50–170 ms was satisfied in the target circle. A liquid reward was given to the animal after each movement. The monkey made five movements to each of the eight targets in a random block design. After completing all 40 trials of the center→out task, the monkey performed drawing tasks in which it traced spirals and figure-eights, the results of which are discussed in the two subsequent papers. This sequence was repeated with each isolated unit.

### *Cortical recording technique*

A 19-mm-diam stainless steel recording chamber was implanted in the skull over the proximal arm region of primary motor cortex. Each day a Chubbuck microdrive (Mountcastle et al. 1975) was mounted on the chamber, which was sealed hydraulically. An electrode, held by the microdrive, was placed over a particular cortical location with an *x-y* stage. *Trans*-dural penetrations were used, and every attempt was made to record cell activity in all layers of the cortex. Single cells were isolated extracellularly with glass-coated platinum-iridium microelectrodes (10-$\mu$m tips). Standard criteria for single-unit identification based on wave shape, its stability, and the absence of doublets or triplets were used (Georgopoulos et al. 1982; Mountcastle et al. 1969) as an indication of a well-isolated, healthy unit. In addition to its activity pattern during the task, the cell's activity was monitored as the joints of the arm were passively manipulated. Small electrolytic lesions (2–3 $\mu$A for 3–5 s) were occasionally placed along a penetration to mark the location of the electrode track for later use during histological identification. Spikes were transduced with a window discriminator to a transistor-transistor logic (TTL) pulse. A clock in the laboratory interface (CED 1401) was used to label the occurrence time of each spike (1-ms resolution) relative to the beginning of the hold-A period. The interface transferred the data to a laboratory microcomputer that controlled the touchscreen display and recorded the finger's position every 20 ms. These data were written to disk between trials.

### *EMG recording technique*

EMGs of various shoulder and upper-arm muscles (*latissimus dorsi; infraspinatus;* posterior, middle, and anterior *deltoids; clavicular pectoralis; triceps; biceps;* and *brachialis*) were performed in a subset of the recorded trials. Two different types of EMG electrodes/

methods were used in this study. The first involved daily placement of fine wire intramuscular electrodes (40 AWG stranded stainless steel) into the five muscles chosen for that day. Each muscle was implanted with two wires (1 cm separation) for bipolar recording. In a different monkey, chronic epimysial patch electrodes (Loeb and Gans 1986) were used. Two stainless steel wires were stripped of their last 5 mm of insulation, threaded through a 7 × 10–mm piece of reinforced Silastic sheeting (spaced 3 mm apart), and bonded to the sheeting using Silastic cement. The epimysial electrodes were surgically implanted under the skin and over the desired muscle belly. The leads to each electrode were routed under the skin to the back of the head where they were attached to a connector and glued to the skull. The raw EMG signals were differentially amplified, band-pass filtered, rectified, and smoothed using a Paynter filter ($\tau = 50$ ms) (Gottlieb and Agarwal 1970) before being sampled at 100 Hz by the laboratory interface (CED 1401). Cross-correlation between a raw rectified EMG and a Paynter filtered EMG showed that the filtered relative to the unfiltered data were delayed by 18 ms. The timing of the Paynter-filtered EMG data used in this study was adjusted accordingly.

### *Cortical activity model*

Although cortical activity is related to several movement parameters, in this study only two of these parameters will be investigated: movement speed and direction. The proposed temporal model of single-cell activity in motor cortex is

$$D(t - \tau) - b_0 = \|\vec{V}(t)\|(b_n + b_y \sin[\theta(t)] + b_x \cos[\theta(t)]) \quad (1)$$

where $D$ is the instantaneous cortical activity, $\tau$ is the time interval between the signal represented in the cortex and its expression as movement, $b_0$, $b_n$, $b_x$, and $b_y$ are constants, $\theta$ is the movement direction, and $\vec{V}$ is the velocity of the finger. The basis for our choice of terms in this equation was developed with a set of initial analyses to separate direction and speed effects on the discharge rates. The validity of the model was then tested with multiple regression.

### *Speed analysis I*

The first step in the data analysis was to identify movement onset in each trial of the center→out task. The position data sampled from the touchscreen were digitally filtered using a phase-symmetric natural B-spline (quintic order) with a low-pass cutoff frequency of 10 Hz (Woltring 1986). Velocity profiles were generated directly from the spline coefficients. Movement onset was defined as the point in time at which the velocity profile rose above 15% of maximum. Because positional data collection ceased as the finger crossed the outer boundary of the target, a portion of the descending velocity profile was truncated. Movement time was then defined as the period between movement onset and subsequent entry into the outer perimeter of the target circle. Reaction time was defined as the period between target circle appearance and movement onset.

The movement time for each trial of the center→out task was divided into 10 bins. In addition, 15 "prebins" were defined in the period just before movement onset. The prebins were used to encompass the neural activity occurring during the hold-A and reaction times. Each prebin had the same time width as a movement bin, and fractional intervals (Richmond et al. 1987; Schwartz 1993) were calculated throughout all 25 bins. The firing rates in each bin were averaged across the five repetitions and square-root transformed (Ashe and Georgopolous 1994). The square-root transform is useful in making the variance of a Poisson distribution (typically found in binned data) independent of its mean (Sokal and Rohlf 1995). (Note: all references to cortical activity in the text and equations assumes the square-root transform has been applied.)

The same 10-Hz low-pass digital filter used for the movement data was applied to the neural data. The firing rate averaged over the last five prebins of the hold-A period (before beginning of reaction period) was calculated and subtracted from each of the 25 bins to remove the tonic background component. Processed firing rates for a single cell were added bin-by-bin across all eight targets to reveal the nondirectional component of the discharge rate profile. This technique is summarized in *Eq. 2*

$$NDD(t) = \sum_{j=1}^{\text{num targets}} [D_j(t - \tau) - b_0] \quad (2)$$

The nondirectional discharge residual (NDD) is the $b_n$ term of *Eq. 1* and can be visualized as a profile similar in shape to, but separated temporally from, that of finger speed. The finger speed recorded during the reaction and movement time was compared with a similar sized time window of neural activity. This window was displaced backward in single-bin time increments through the entire neural profile. Correlations were taken at every step and the lag at which the highest correlation occurred was deemed the average lag, $\tau$, for that cell.

To generate an ensemble representation of speed, the nondirectional components of all recorded cells were averaged together binwise. An overall lag was calculated from the ensemble representation using the sliding window correlation method described above. As a comparison to neural activity, a similar ensemble analysis was carried out on the EMG data.

### *Directional analysis*

Initially, a single, mean firing rate was calculated over the reaction and movement times for each trial, averaged over the five repetitions to each target, and square-root transformed. The finger location at the end of movement time was subtracted from its location at movement onset, yielding a movement displacement vector that was averaged over the five repetitions to each target. The directional components of the averaged displacement vectors and the cortical activity were regressed to the cosine tuning function model

$$\bar{D}_j = B_0 + B_y \sin \bar{\theta}_j + B_x \cos \bar{\theta}_j \quad (3)$$

$\bar{D}_j$ is the estimated discharge rate during the movement to target $j$, $\bar{\theta}_j$ is the direction of finger movement, and $B_{0,x,y}$ are the regression coefficients. The bars above the variables in *Eq. 3* represent time averages taken over the reaction and movement times. Taking time averages and assuming the velocity profile to each target is equal, it can be shown that *Eq. 1* reduces to *Eq. 3* because the speed term ($b_n$) in *Eq. 1* can be combined with the $b_0$ term to yield the $B_0$ in the above equation. Applying the regression model to each cell generated a "preferred direction" for the cell as well as a coefficient of determination ($r^2$) corresponding to the "fit" of the model (Georgopoulos et al. 1982). The EMG activity occurring over the reaction/movement period was also averaged and directionally analyzed using *Eq. 3*, yielding a preferred direction for each muscle recorded in this study.

Once the nondirectional component of the cell's activity was found, it was subtracted from the total discharge pattern along with the tonic activity to get an estimate of the time-varying directional component to each target. According to *Eq. 1*, the directional component of a cell's firing rate for the center→out task ($b_y$ and $b_x$ terms when multiplied by $\|V(t)\|$) should be a series of bell-shaped curves in time. Movements to the target closest to the cell's preferred direction should generate the largest positive curve. Conversely, the directional component of discharge for movements opposite the preferred direction should be a negative curve whose magnitude is equal to that seen in movements in the preferred direction. Movements to the remaining targets should generate directional components with magnitudes that vary systematically between those in the preferred and anti-preferred direction. The directional components to each of the eight targets were categorized according to the angle between the movement direction

and the cell's preferred direction. The data in each category (0, ±45, ±90, ±135, 180) were averaged over all cells to obtain ensemble temporal representations of the directional components.

### *Speed analysis II*

Whereas *Eq. 1* will give a firing rate profile in time, it is also informative to examine the effect of speed on the directional tuning function (discharge rate vs. direction). For this analysis we used average discharge rates during trials in which the movements were of different durations. The behavioral paradigm did not completely constrain the speed used by the monkey to reach each target; it was rewarded for movement durations <300 ms. Because of the extensive amount of training before recording data and because our analysis is based on five-repetition averages, ensemble intertarget variations in speed were not significant. However, by analyzing individual repetitions, enough variation in intratarget speed was found to make some statistically significant observations. This allowed us to construct directional tuning functions for different movement speeds.

To compensate for the latency between cortical activity and finger speed, the average time lag, $\tau$, found previously was used to select the 10 bins of cortical activity that corresponded to finger movement. Because there is significant variation in firing rate magnitudes across different cells, the individual firing rates ($n = 40$) for each cell were normalized by their overall mean. Each of the targets for a particular cell were labeled according to its direction relative to the cell's preferred direction. The normalized firing rates for movements in the cells' preferred directions were regressed to peak finger speeds. This provided a measure of the change in overall firing rate due to changes in speed when moving in the average cell's preferred direction. This was repeated for movements ±45, ±90, ±135, and 180° from the preferred direction. Combining these results, the variation in the "average" tuning curve as a function of speed was found.

The same analysis was applied to the EMG data to calculate the effect of finger speed on the muscle tuning curves. To combine multi-day data for the same muscle, the baseline voltage from each experiment was subtracted before analysis.

### *Population vector analysis*

The population vector algorithm (Georgopoulos et al. 1983) uses each cell's preferred direction to define a vector that is subsequently weighted by its current activity and summed with vectors similarly derived from other cells recorded during the same task. The resultant vector, termed the "population vector," tends to point in the direction of movement. A time series of these vectors can be generated throughout the movement, and they match the instantaneous velocity of the hand as it moves (Georgopoulos et al. 1988; Schwartz 1993). This algorithm can be expressed in equation form as

$$PV_{y,j}(t) = \sum_{i=1}^{\text{num cells}} \frac{D_{i,j}(t-\tau) - A}{M} \cdot \frac{B_{y,i}}{M} \qquad (4)$$

$PV_{y,j}(t)$ is the $y$ component of the population vector (predicted velocity vector) at time $t$ for target $j$. $A$ is a bias term that centers the cell's firing rate about zero. In a task that has balanced velocity components (speed and direction) such as the center→out task, $A$ is typically set to the average firing rate $B_0$. However, in an unbalanced movement task (i.e., essentially any figure whose shape is not identically symmetrical about all axes), $A$ is set to the geometric mean of the temporal firing rate. $M$ is a normalization factor that scales the cell's maximum firing rate to unity. The direction coefficient (found from a regression of *Eq. 3*) for the $i$th cell in the $y$ direction is $B_{y,i}$. The $x$ component of the velocity vector is calculated by substituting $B_{x,i}$ as the direction coefficient.

## RESULTS

A total of 1,066 cells were recorded from eight hemispheres of four monkeys. Figure 1 illustrates the locations of the 218 penetrations from which these cells were recorded. In seven of the eight hemispheres, recordings were made in the primary motor cortical area; in one hemisphere dorsal premotor activity was recorded exclusively. The criterion used to select cells for further analysis was that good single-unit isolation was maintained during all five repetitions to each of the eight targets (40 trials). Each unit was examined during passive manipulation of the shoulder, elbow, wrist, and hand. Cells that were responsive exclusively to manipulation of the hand or fingers were excluded from further analysis. These criteria were met for 1,039 of the units, 142 of which were recorded in dorsal premotor cortex. The major purpose of this analysis was to study primary motor (M1) cortical activity. However, as a comparison, a limited number of dorsal premotor (Pmd) cortical cells were similarly analyzed.

The average trajectories to each of the eight targets over all trials are shown in Fig. 2*A*. The circle sizes (1 cm radius) representing the targets, excursion lengths, (6 cm) and trajectories are drawn to scale. The thick lines are average trajectories comprised of 5,195 movements to each target. Standard deviations are represented by the thin lines. Movement recording was initiated at the beginning of the reaction time (interval between peripheral target presentation and movement initiation) and ended when the outer perimeter of the target circle was crossed. The average velocity profiles to each of the eight targets (thick lines), and the overall standard deviation (thin lines) across all recorded trials are shown in Fig. 2*B*. An ANOVA (IMSL, Visual Numerics) on the peak speeds grouped by targets found that these speeds were not significantly different across targets ($p < 1\%$).

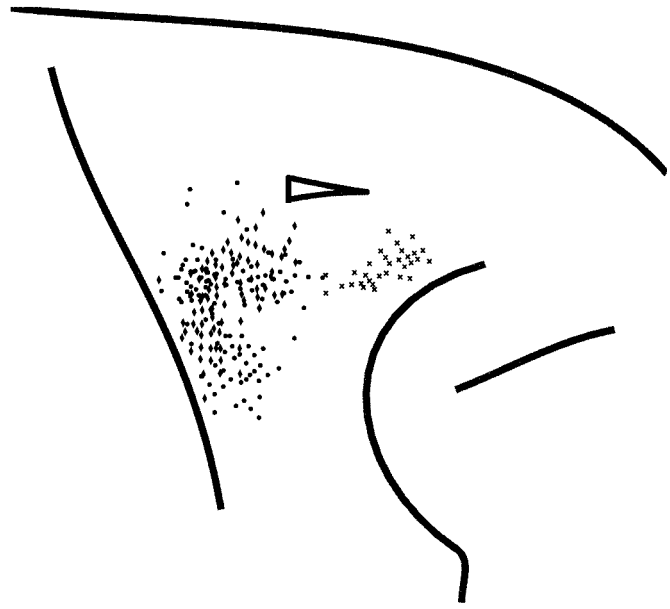

FIG. 1. Electrode penetration locations from 8 hemispheres of 4 monkeys. Recordings in 7 of the 8 hemispheres were in primary motor cortex (● and ◆). One set of recordings was made in dorsal premotor cortex (×). ◆ and ×, penetration sites of the cells also analyzed in the 2nd and 3rd paper.

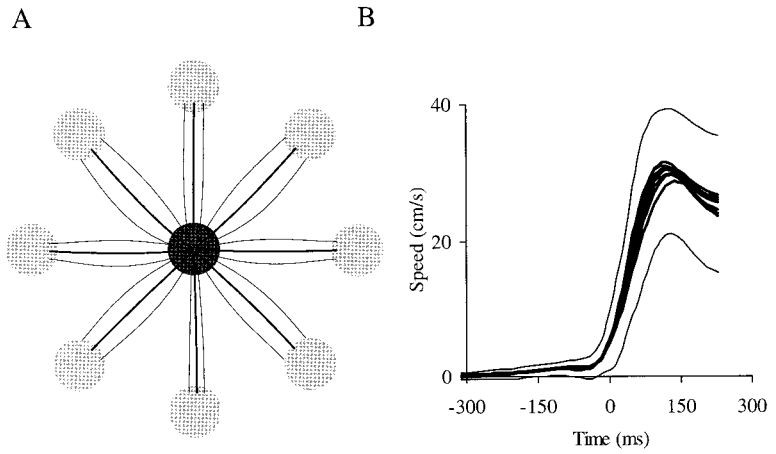


FIG. 2. Average movement kinematics for the center→out task. *A*: the monkey placed its finger in the center start circle (dark gray circle) and made a planar movement to one of the 8 peripheral targets (light gray circles). The thick black line shows the average of 5,195 movements to each target. The thin lines represent the standard deviation of the mean. *B*: average velocity profiles to each of 8 peripheral targets are shown by the 8 thick black lines. The overall standard deviation (across all target directions) is represented by the thin lines.

*Speed response I*

The neuronal firing rates during each trial's movement time were divided into 10 bins to normalize binwidths among all trials. Across all cells, the average binwidth was 24 ± 5 (SE) ms for 41,560 trials. In addition, 15 prebins, having the same width as the movement bins, were calculated just before movement onset. On average, the first eight bins corresponded to the later part of the hold-A period, and the next seven bins covered the reaction time. Five-trial averages were made over all movement directions. The outer perimeter of Fig. 3 shows the raw (i.e., unsmoothed and untransformed) firing rates during movements to each target for an example cell. During the hold-A period the rates were very similar across targets. In the subsequent reaction and movement times, the activity was graded with movement direction.

These histograms were smoothed and square-root transformed. The average firing rate in the five bins before reaction time was subtracted from the reaction and movement time bins, eliminating the tonic component of cortical activity ($b_0$). Averaging the resulting profiles across the eight targets removed the directional component ($b_x$ and $b_y$ terms) of the discharge profile. Finally, the 17-bin window of neural activity that best correlated with finger speed over the reaction and movement time was found. The result is the left profile in the center of Fig. 3. This nondirectional profile is very similar to the speed of the hand averaged across the eight targets (right profile in the center of Fig. 3). For this cell, the two waveforms were highly correlated ($r^2 = 0.96$) at a lag of 155 ms. In general, this was true for cells throughout the motor cortical population as shown in Fig. 4A. A histogram of the corresponding time lags between the nondirectional discharge and velocity profile for all M1 cells in the population can be seen in Fig. 4*B*. The time lag distribution peaked at a mode of 125 ms with a median value of 75 ms.

A similar analysis was performed on the recorded responses of 142 premotor cortical cells. Figure 4*C* shows the results of correlating the nondirectional portions of Pmd cortical discharge with speed. Lags between Pmd cortical activity and finger speed had a median value of 100 ms, but the mode of the distribution was 175 ms (Fig. 4*D*).

An ensemble nondirectional activity profile was generated by averaging all 897 M1 profiles bin-by-bin. The result (Fig. 5) is highly correlated ($R^2 = 0.99$) with the speed profile, and leads it by 145 ms. This M1 profile was compared with those derived from Pmd and muscle activity. Each curve in Fig. 5 is composed of the 17 bins that best correlate with finger speed. Pmd activity had an $r^2$ of 0.68 at a lag of 190 ms. Nondirectional EMG activity was also correlated to the speed profile ($R^2 = 0.96$, lag = 65 ms).

*Directional response*

Figure 6 shows the response of a motor cortical cell (same cell as Fig. 3) during the center→out task. The firing rate

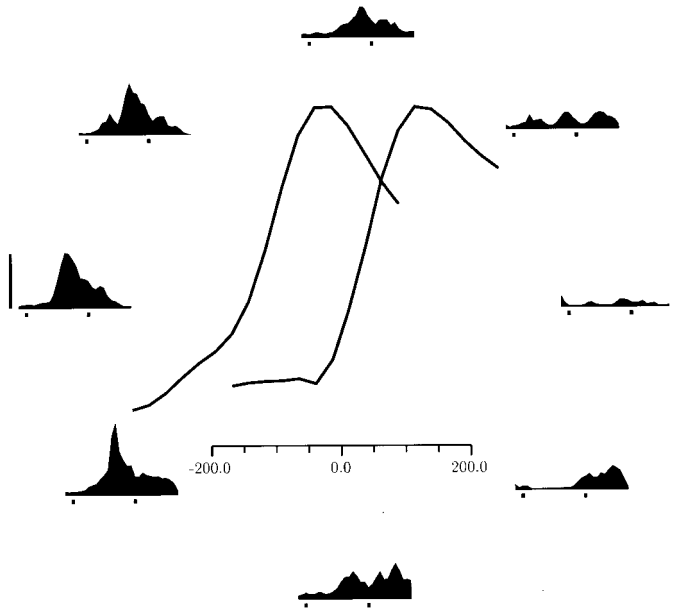


FIG. 3. Speed representation in a motor cortical cell. Firing rates for movements to each of the 8 center→out targets were aligned to movement onset ($V > 0.15V_{max}$), divided into 25 bins (26-ms binwidth) and averaged over 5 trials. The resulting histograms, located radially around the figure, represent the average cortical activity recorded for movements in each of the respective directions. The vertical calibration bar on the left of the figures represents 100 spikes/s. The timing marks under each histogram are 440 ms [average reaction time (RT) + movement time (MT)] apart and represent the portion of the histogram that was used to generate the central figure. These firing rates were then smoothed using a 10-Hz low-pass digital filter and square-root transformed. The tonic firing rate occurring during the hold-A period (i.e., the activity before the 1st timing mark in the histograms) was subtracted from the record. The firing rates were then summed over the 8 movement directions to cancel the directional component. The resulting nondirectional profile (*left middle*) is highly correlated to the average movement speed (*right middle* profile).

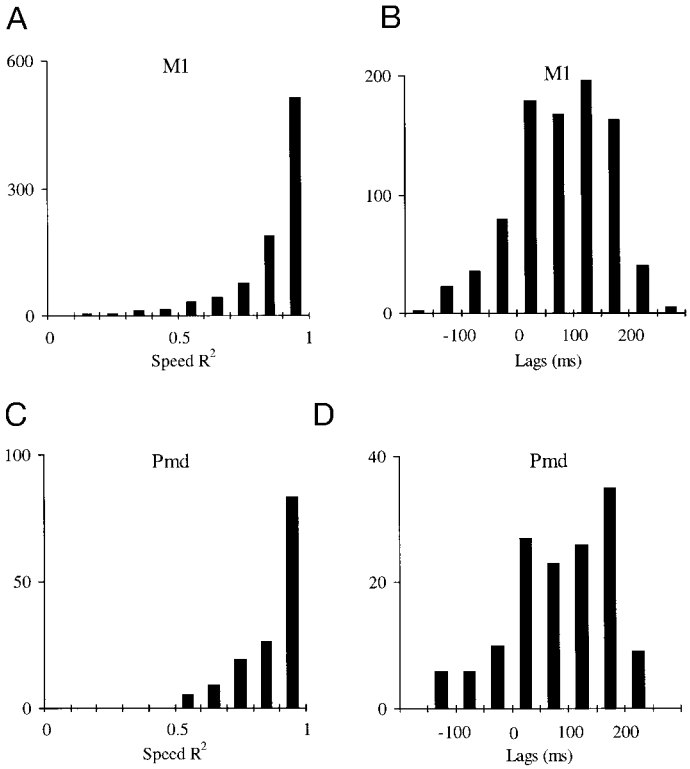


FIG. 4. *A*: histogram of maximum $r^2$ values between actual movement speed and neural nondirectional component from 897 M1 cells. A sliding time window equal to the RT + MT was used to find the maximum $r^2$ for each cell. *B*: lags between M1 cells' nondirectional components and the actual movement speeds as determined from peak correlations of the sliding window analysis (*A*). *C* and *D*: same analyses applied to the 142 dorsal premotor (Pmd) cells.

during the reaction and movement times to each target was averaged temporally over the trial and across repetitions. The eight resulting firing rates were square-root transformed and regressed against direction (*Eq. 3*) to generate a directional tuning function. The filled circles in the polar plot of Fig. 6 represent the processed firing rates for the cell, and the solid black line is the cosine tuning function. The tuning function explains well the dispersion of these points. The $r^2$ for the directional tuning of this cell is 0.96 with a preferred direction of 180° (arctan[$B_y/B_x$]).

All cells used in this study were analyzed this way. A

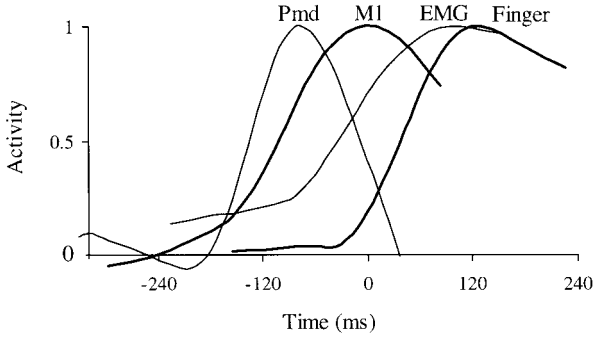


FIG. 5. Average representation of nondirectional components in muscles and cortical cells. The finger speeds ($n$ = 41,560) of all recorded trials were averaged over reaction and movement times (*rightmost profile*). Ensemble nondirectional components for Pmd ($n$ = 5,680), M1 ($n$ = 35,880), and electromyographic recordings (EMG; $n$ = 8,800) were correlated to movement speed using a sliding window analysis.

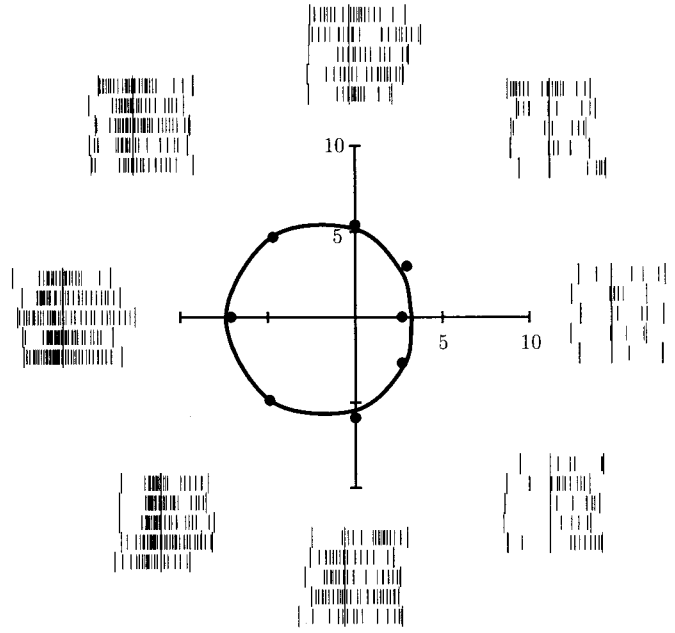


FIG. 6. Directional tuning in a motor cortical cell. The outer raster data show the spike activity occurring between the beginning of reaction time (1st long hash mark) and the end of the movement (last long hash mark). The firing rates for movements to each target were temporally aligned to central target exit time (center long hash mark) and square-root transformed. The center polar plot shows the resulting average firing rates for each target (●) regressed to a cosine function (—). The units on the polar plot are in [rad]spikes/s.

histogram of $r^2$ values for the 1,039 cells is shown in Fig. 7*A*. (Note: due to their similarities in directional tuning, both Pmd and M1 responses were included in Fig. 7.) The average $r^2$ was 0.71 with 75% having values greater than or equal to 0.7. The distributions of preferred directions can be seen in the circular histogram of Fig. 7*B*. Preferred directions were well distributed throughout the workspace with a very slight skewing. The 0° bin (rightward) of preferred directions contained the highest number of cells (101). The direction with the least number of cells (70) was down and to the left (240°). All other directions contained counts between 70 and 101 cells. A Rayleigh test (Batschelet 1981) performed on the preferred directions resulted in a test statistic of $z$ = 0.45, which corresponds to a $p$ value = 0.64. The null hypothesis of a uniformity cannot be rejected, and there is little uncertainty that this distribution is uniform.

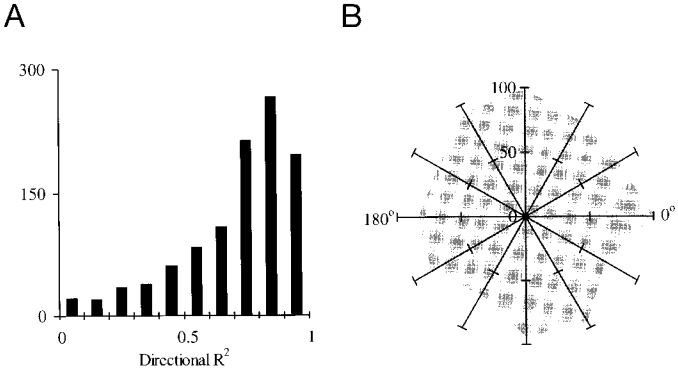


FIG. 7. *A*: histogram of directional tuning $r^2$ values for 1,039 cortical (M1 and Pmd) cells. *B*: distribution of preferred directions in the tested work space. A circular histogram composed of 30° bins shows a maximum count of 101 in the 0° bin and a minimum count of 70 in the 240° bin.

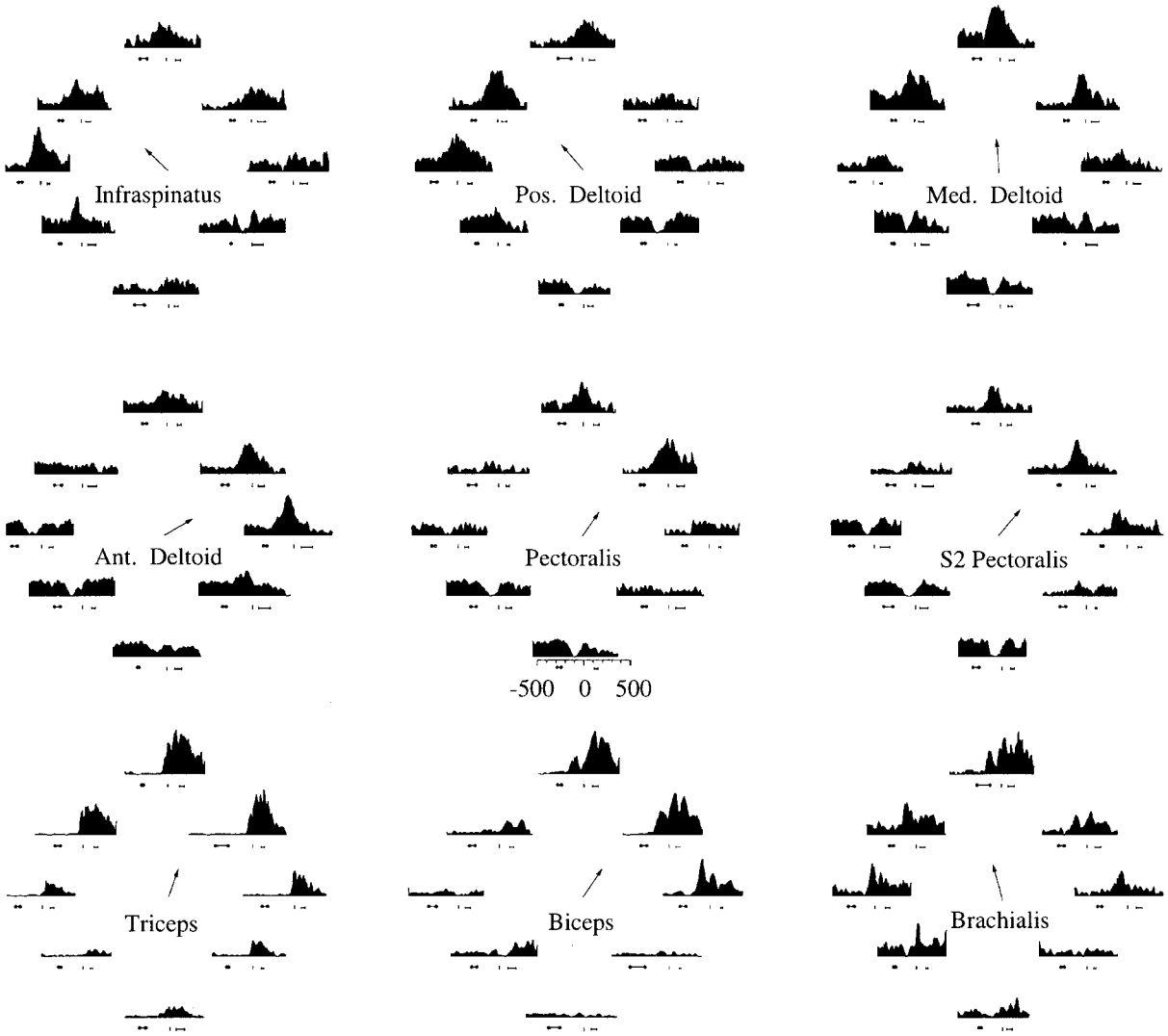


FIG. 8. Directional tuning in shoulder/elbow muscles. The temporal activities to each of the eight targets are positioned accordingly in each figure with the muscles' "preferred directions" shown in the center of each figure. The 5-trial histograms were aligned by central target exit. The range of reaction time onsets (●) and the range of movement terminations (vertical bars) are shown beneath each histogram. All muscles with the exception of "S2-Pectoralis" were recorded from the same arm.

Similarly, the average EMG activity of each muscle was directionally analyzed. Figure 8 shows the temporal activity of nine of the left arm muscles recorded in this study. Except for the "S2 Pectoralis," all the examples shown in Fig. 8 were from a single monkey (S1) using intramuscular electrodes. Beginning with the *top row*, a systematic rotation in preferred directions can be seen in the shoulder muscles whose origins vary systematically from posterior to anterior. Note the similarity in preferred directions between the two pectoralis muscles shown in Fig. 8, suggesting that the two monkeys used very similar strategies in controlling this muscle. Another interesting result in Fig. 8 is the similarity in preferred directions among the biceps and triceps from the same arm. Classically considered antagonists to one another, these two muscles appear to be co-contracting during movements up and to the right. However, on closer inspection it can be seen that the biceps activity precedes the triceps activity. The biceps crosses the shoulder, and the short head acts as a shoulder flexor in addition to its contribution to elbow flexion. The early activity in this muscle may be acting to flex the shoulder. The subsequent uniarticular triceps activity (short and lateral heads) counteracts elbow flexion and allows the biceps to continue flexing the shoulder. Although the triceps long head does cross the shoulder, its primary function is stabilization of the shoulder joint, and it contributes insignificantly to shoulder flexion/extension (Gray's Anatomy 1980).

EMG activity from 14 left arm muscles of 2 different monkeys was recorded. The number of trials recorded for each muscle varied. Table 1 shows the total number of trials recorded for each muscle, those trials with significant directional tuning and the average preferred direction across tuned trials. A histogram of $r^2$ values for directional tuning in muscles (Fig. 9*A*) shows that the EMG activity was as well tuned as that of the neurons during this task. However, Fig. 9, *B* and *C*, graphically compares the average preferred directions among the muscles recorded and shows that almost all of them are orientated upward and within 45° of the vertical axis. The Rayleigh test yields a statistical value of 8.70, which corresponds to a $p$

TABLE 1. *Directional tuning statistics of EMG activity recorded from the left arms of two monkeys*

| | *Subject 1*, Left Arm | | *Subject 2*, Left Arm | |
|---|---|---|---|---|
| | All PD | Tuned PD | All PD | Tuned PD |
| Infraspinatus | 137 (1) | 137 (1) | 114 ± 7 (15) | 114 ± 7 (15) |
| Posterior deltoid | 137 ± 45 (34) | 129 ± 53 (27) | 185 ± 16 (15) | 188 ± 34 (13) |
| Middle deltoid | 125 ± 29 (33) | 130 ± 56 (23) | 114 ± 21 (15) | 108 ± 32 (13) |
| Anterior deltoid | 57 ± 21 (7) | 57 ± 21 (7) | | |
| Pectoralis | 54 ± 41 (18) | 54 ± 50 (16) | 49 ± 5 (15) | 49 ± 5 (15) |
| Triceps | 71 ± 25 (31) | 71 ± 74 (14) | | |
| Biceps | 91 ± 54 (3) | 62 ± 52 (2) | | |
| Brachialis | 97 ± 19 (10) | 98 ± 33 (9) | 59 ± 37 (15) | 74 ± 94 (4) |
| Latissimus dorsi | 61 ± 13 (8) | 59 ± 44 (6) | | |

Values are means ± SE with total number of trials in parentheses. For each subject, the average preferred direction (PD) and standard deviation (SD) are tabulated for all the trials recorded for that muscle as well as for only the tuned trials ($r^2 > 0.7$).

value of 0.00017. The null hypothesis of uniformity is clearly rejected. This differs from the distribution of cortical cell preferred directions, which were found to be uniform (Fig. 7*B*).

Starting with the activity profiles of individual cortical cells, directional (corresponding to the $b_x$ and $b_y$ terms in *Eq. 1*) and nondirectional (the $b_n$ term) activity patterns were separated by

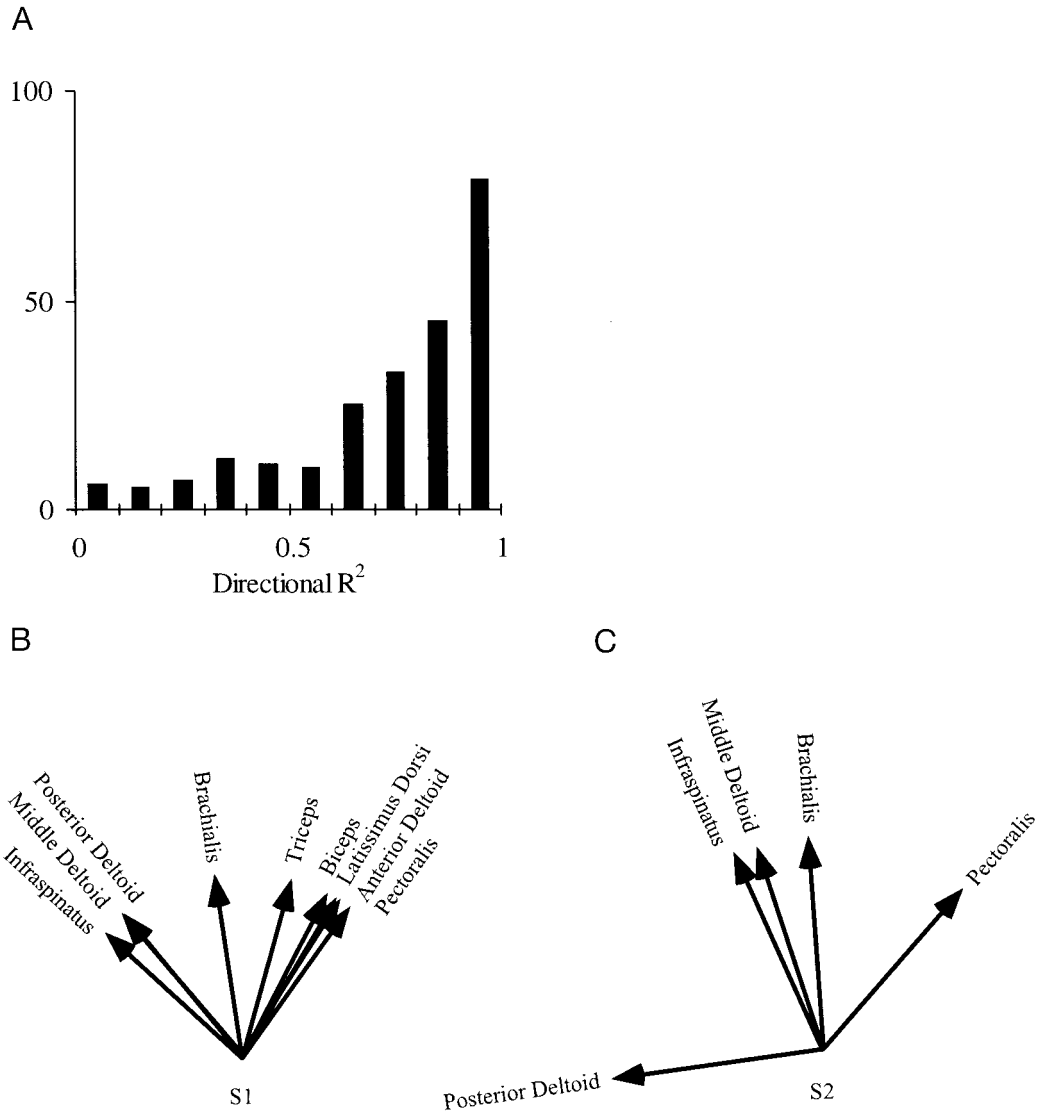


FIG. 9. *A*: histogram of directional tuning $r^2$ in muscles ($n = 220$ experiments, 14 muscles). *B*: distribution of average preferred directions of 9 left arm muscles from a single monkey (*S1*). All of the muscles have significant upwards "tuning." *B*: distribution for the 5 left arm muscles of a different monkey (*S2*). With the exception of posterior deltoid, all these muscles are also tuned upward.

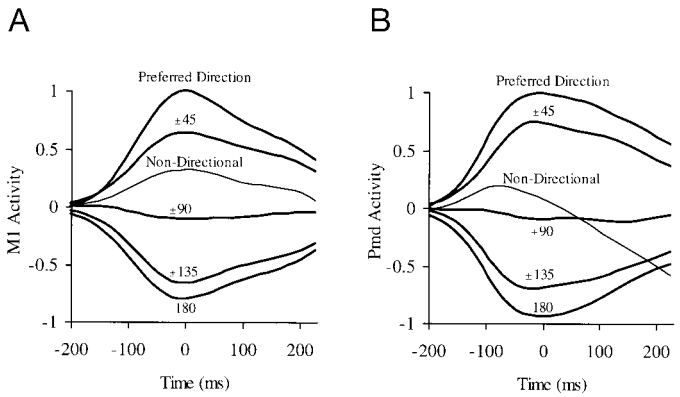


FIG. 10. *A*: average representation of directional coding in M1 cells. Each cell's tonic and nondirectional components were subtracted from the overall firing rate profile recorded during a movement to a single target. The resulting directional component for each target was categorized relative to the cell's preferred direction. Directional components derived from movements closest to the cells' preferred directions were averaged across all cells in the population and can be seen as the uppermost thick line. Those components from targets that were ±45, ±90, ±135, and 180° away from the cells' preferred directions can be seen as the next 4 solid lines, respectively. Finally, the nondirectional component from Fig. 5 can be seen as the thin line. *B*: similar procedure performed on the Pmd cells. *Time 0* represents movement onset.

subtracting both the tonic and nondirectional activity to each target. These profiles were then categorized by preferred direction and averaged across cells to give the average directional components to each target (relative to preferred direction) across the population. The average nondirectional response (same as Fig. 5) is shown together with the directional profiles in Fig. 10*A*. When moving in the preferred direction, the M1 directional component is much larger than the nondirectional term. In contrast, when moving perpendicular to the preferred direction, the time-varying directional component is very small, suggesting that the observed activity of a cell is dominated by the nondirectional component when moving in this relative direction. With the exception of ±90°, the directional and nondirectional components have similar bell-shaped profiles, suggesting that both terms could contain instantaneous speed information. This is the rationale for setting the speed term in *Eq. 1* as a multiplier to both the directional and nondirectional terms.

The directional interprofile amplitudes shown in Fig. 10*A* begin following the cosine tuning model ~50 ms into the reaction time. From that point on, the correlation with the tuning model remains high ($r^2 > 0.98$) throughout the rest of the movement. However, the profile amplitude for movements in the preferred direction (*top curve*) has a larger overall magnitude than in the anti-preferred direction (*bottom curve*). Because these curves were derived by subtracting the same nondirectional component from the response to each target, this may indicate that the speed component varies (interacts) with movement direction. In fact, previous work (Schwartz 1992) has shown that speed is better represented in motor cortical activity patterns when movements are near the cell's preferred direction. Subtracting a constant contribution from each profile would then tend to underestimate the speed component for the profiles near the preferred direction, making the resulting direction profile too large.

The nondirectional response in the premotor population appears to have a much faster temporal profile than both the finger speed (Fig. 5) and the directional responses (Fig. 10*B*). The directional interprofile magnitudes from the premotor ensemble show excellent cosine tuning ($r^2 > 0.99$) throughout the movement illustrating that premotor cell activity can represent direction very well.

TABLE 2. *Results from regressing primary motor cortical (M1) and dorsal premotor (Pmd) activity ($\sqrt{spikes/s}$) with finger speed (cm/s) for various directions relative to cells' preferred directions*

| Direction | Mean Rate | Slope | CC | DOF | Significant (5%) | Ratio |
|---|---|---|---|---|---|---|
| | | | *M1 cells* | | | |
| 0 | 1.26 | 0.015 | 0.38 | 4,463 | yes | 0.12 |
| 45 | 1.16 | 0.015 | 0.41 | 8,928 | yes | 0.13 |
| 90 | 0.89 | 0.011 | 0.35 | 8,928 | yes | 0.12 |
| 135 | 0.68 | 0.008 | 0.28 | 8,928 | yes | 0.12 |
| 180 | 0.62 | 0.008 | 0.29 | 4,463 | yes | 0.13 |
| | | | *Pmd cells* | | | |
| 0 | 1.40 | 0.030 | 0.38 | 708 | yes | 0.21 |
| 45 | 1.27 | 0.022 | 0.30 | 1,418 | yes | 0.17 |
| 90 | 0.90 | 0.008 | 0.17 | 1,418 | yes | 0.09 |
| 135 | 0.67 | 0.009 | 0.18 | 1,418 | yes | 0.14 |
| 180 | 0.58 | 0.003 | 0.09 | 708 | yes | 0.05 |

The mean normalized discharge rate, slope of the regression line, correlation coefficient (CC), degrees of freedom (DOF), and significance of the regression are listed consecutively. The slope monotonically decreases but always remains positive as the direction gets further away from the preferred direction. The last column shows the ratio of the change in firing over the mean for moving from 25 to 35 cm/s. Although the absolute slope varies with direction in the M1 ensemble, the ratios (i.e., relative slopes) remain fairly constant suggesting that finger speed scales the tuning function.

### *Speed response II*

Average speed profiles for movements to each of the eight targets were statistically similar across targets. However, magnitudes of individual profiles vary in repeated movements to the same target. Trials were sorted by movement direction (relative to the preferred direction), and the average discharge rate in each trial was regressed to peak speed. EMG activity

TABLE 3. *Regression results from proximal arm EMG activity $\sqrt{|volts|}$ and finger speed (cm/s)*

| Muscle | Direction | Mean Rate | Slope | CC | DOF | Significant (5%) |
|---|---|---|---|---|---|---|
| Anterior deltoid | 0 | 5.47 | 0.183 | 0.38 | 33 | yes |
| | 45 | 3.95 | 0.171 | 0.44 | 68 | yes |
| | 90 | 0.89 | 0.086 | 0.42 | 68 | yes |
| | 135 | −2.08 | −0.052 | −0.19 | 68 | no |
| | 180 | −2.97 | −0.081 | −0.23 | 33 | no |
| Infraspinatus | 0 | 2.42 | 0.031 | 0.34 | 73 | yes |
| | 45 | 1.88 | 0.003 | 0.22 | 148 | yes |
| | 90 | 0.95 | 0.001 | 0.04 | 148 | no |
| | 135 | 0.09 | 0.004 | 0.08 | 148 | no |
| | 180 | −0.27 | 0.006 | 0.32 | 73 | yes |

Only those muscles that had significant correlations in the preferred direction (0) and at least one other direction are listed. The mean rate in the table is from the phasic activity of the muscles (i.e., activity during hold-A period has been subtracted from entire record). The slopes are large and positive in the preferred direction but quickly drop to zero or become negative. CC, correlation coefficient; DOF, degrees of freedom.

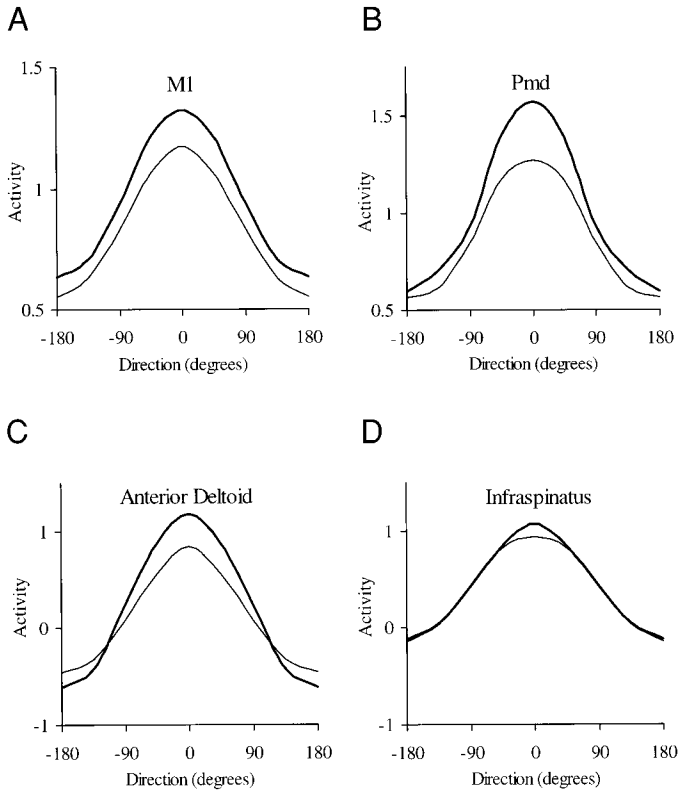


FIG. 11. Cortical and EMG tuning functions for different finger speeds. These functions were constructed from the results of regressing finger speed with normalized activity (Tables 2 and 3). In all figures, the thick black curve represents normalized activity during movements made with a peak speed of 35 cm/s. The thinner line corresponds to a peak speed of 25 cm/s. For the cortical figures (*A* and *B*), the center of the tuning curve for the mean speed (30 cm/s) is represented by an ordinate value of 1.0. For the muscular data, an ordinate value of 0.0 represents tonic activity during hold-A period, and 1.0 represents muscular activity when moving at mean speed in the muscle's preferred direction. *A*: M1 cortical activity is always higher for faster speeds regardless of direction. *B*: Pmd cortical activity is also positively correlated with speed. *C*: anterior deltoid activity increases for higher speeds when moving in the muscle's preferred (agonistic) direction; however, this muscle's activity decreases during increasing speed for movements in the anti-preferred (antagonistic) direction. *D*: speed effects infraspinatus activity only when moving near the preferred direction.

was regressed to speed the same way. The regression results that were found to be significant in at least two or more directions are shown in Tables 2 and 3.

The motor cortical regression analysis shows that discharge rate increases with increasing finger speed regardless of finger direction. However, the amount of change in discharge (i.e., slope) is dependent on direction. The discharge rate increases more in the preferred direction than in the anti-preferred direction (Table 2). The mean peak speed in this analysis was ~30 cm/s with a standard deviation of ±10 cm/s. The mean rate and slopes for each direction were used to construct ensemble tuning curves for trials with peak speeds of 25 and 35 cm/s (Fig. 11*A*). The difference in firing rate between the two curves is greater in the preferred direction than in the anti-preferred direction, suggesting that speed does not simply shift the tuning curve. The ratios (last column of Table 2), consisting of the differences between fast and slow firing rates divided by their mean, were similar across directions, suggesting that the speed effect was multiplicative on the directional tuning curve.

The premotor cortical cells also showed an overall increase in discharge rate with increasing finger speed, which was significant throughout all directions. However, the change in discharge rate was twice as large as that for the M1 cells in the preferred direction and substantially less in the anti-preferred direction (Fig. 11*B*).

Of the 14 muscles analyzed, only two showed significant changes in activity with increasing speed in two or more target directions (Table 3). EMG patterns for anterior deltoid and infraspinatus were positively correlated with finger speed when moving in the muscle's preferred direction. As movements were made further away from the muscle's preferred direction, the slope between EMG and speed either became insignificant or negative. (Although statistically insignificant, similar patterns were seen in all recorded muscles). The anterior deltoid activity shown in Fig. 11*C* is greater with faster movements when moving upwards (90°). However, because this muscle is active during the hold-A period to counteract gravity, it decreases activity when the arm moves downward (270°). For faster movement speeds in the anti-preferred direction (downward), there is a decrease in anterior deltoid activity instead of an increase. This is opposite the effect seen in motor cortical cells for movements made in the anti-preferred direction (Fig. 11, *A* and *B*). The direction response of infraspinatus was only modulated by speed when moving in the muscle's preferred direction (Fig. 11*D*).

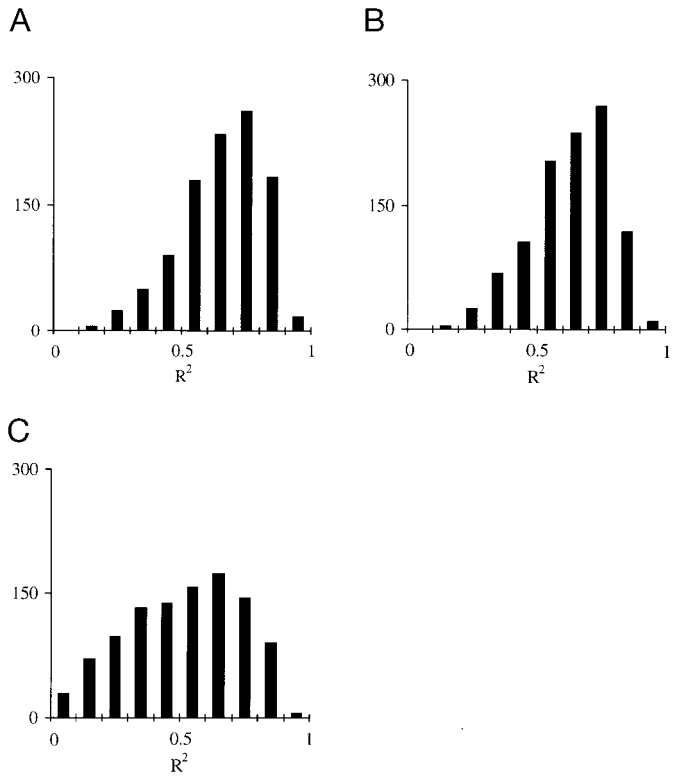


FIG. 12. Results of a multiple regression analysis of *Eq. 1* on single cell data. *A*: histogram of $r^2$ values for all cells ($n$ = 1,039) recorded in this study. *B*: a similar analysis performed on nontransformed firing rates resulted in a slightly poorer median. *C*: using a constant lag of 145 ms, a reduced median $r^2$ value was found for the transformed data.

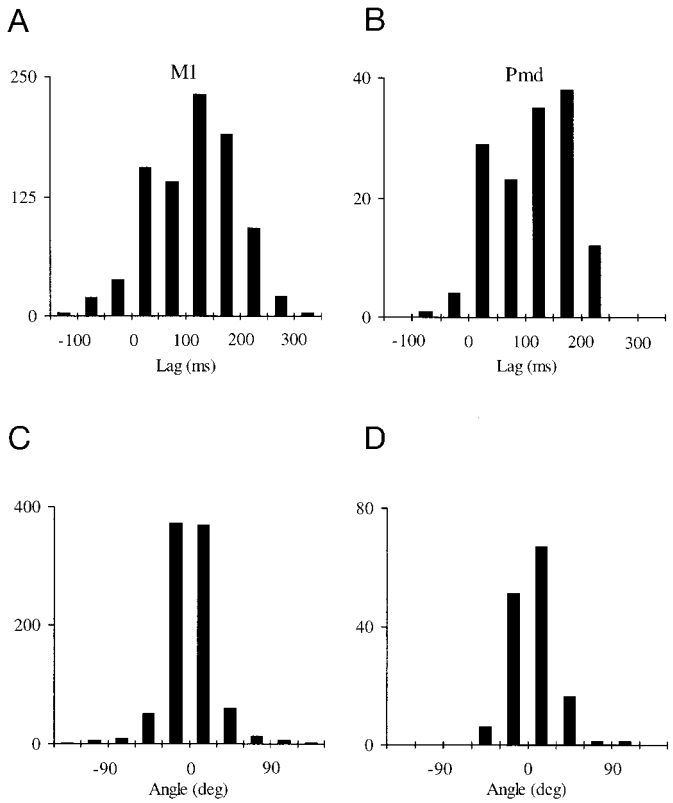


FIG. 13. *A* and *B*: histograms of time lags found from the multiple regression analysis of *Eq. 1* on the primary motor cortical cells (*A*) and dorsal premotor cells (*B*). The distributions of lags are very similar to those shown in Fig. 4. The dynamic data from the regression shown in Fig. 12*A* (*Eq. 1*) were used to calculate preferred directions, and these were compared with the conventional, time-averaged calculation of preferred direction (*Eq. 3*) in *C* and *D*. The 2 methods gave similar results with >80% of both the primary motor (*C*) and premotor (*D*) cortical cells falling within a difference angle of <30°.

### *Multiple regression*

*Equation 1* was validated using a multiple regression analysis (rcov − IMSL). The form of *Eq. 1* used in the multiple linear regression is

$$D(t-\tau) = b_0 + \|\vec{V}(t)\|b_n + \|\vec{V}(t)\|b_y \sin[\theta(t)] + \|\vec{V}(t)\|b_x \cos[\theta(t)] \quad (5)$$

The discharge rate, finger velocity, and direction as a function of time were the known parameters of the regression. The time lag ($\tau$) was varied from 250 to −125 ms in single bin increments. Two separate regressions were performed on each cell; one in which the firing rates were square-root transformed and the other in which they were not. Figure 12 shows the histograms of $r^2$ values for all cells recorded ($n$ = 1,039) under three different conditions. Because this is a temporal analysis, the degrees of freedom (DOF) in the regression of *Eq. 1* is much higher (78 DOF) than the time-averaged regression of *Eq. 3* (6 DOF). As a result, an $r^2 > 0.08$ is statistically significant at the $p$ = 1% level. In Fig. 12*A*, the time lag that yielded the best fit to the model (i.e., highest $r^2$) for each cell using square-root transformed data were used to build a histogram of $r^2$ values. Figure 12*B* is a similar analysis performed on nontransformed data. Finally, Fig. 12*C* shows the histogram for square-root transformed data using a fixed lag of 145 ms. The median $r^2$ values in Fig. 12, *A–C*, are 0.68, 0.65, and 0.54, respectively. The results in Fig. 12, *A* and *B*, are very similar; the square-root transform slightly reduces the variance without changing the shape of the distribution.

The individual cortical lags that provided the best fits to *Eq. 1* can be seen in Fig. 13, *A* and *B*. The figure is divided into primary and premotor cortical subpopulations to compare with the lags shown in Fig. 4, C and *D*. The distributions in Figs. 4, *C* and *D*, and 13, *A* and *B*, have identical modes and very similar shapes showing that the two methods for calculating cortical time lags provide similar results. Figure 13, *C* and *D*, show a distribution of differences in preferred directions calculated from regressing the mean rates of *Eq. 3* and the dynamic rates of *Eq. 1* to cortical activity. The preferred direction is determined by the regression coefficients $b_y$ and $b_x$ (preferred direction = arctan $b_y/b_x$). Less than 20% of the cells had preferred directions that varied by >30° between the two models.

An average representation of cortical discharge rate was generated by categorizing cell activity by preferred direction and averaging across all cells. Using *Eq. 1* to regress the eight temporal firing rates to the corresponding finger velocities, an overall $r^2$ of 0.99 was found at a lag of 145 ms. None of the individual cells had $r^2$ values >0.95, yet over 99% of the variance in the average motor cortical activity can be explained by *Eq. 1*.

### *Population response*

We used the responses of individual cells in the cortical population to provide a measure of how their combination might lead to a representation of speed and direction during reaching. Responses from all directionally tuned ($r^2 > 0.7$) M1 cells were combined to form a time series of population vectors. The results are shown in the perimeter of Fig. 14*A*, where movements to each target are represented by 17 population vectors (7 for RT and 10 for MT) as well as the corresponding movement velocity vectors. Vectors corresponding to each movement are centered at their corresponding target location in the diagram with the time series advancing in a counter-

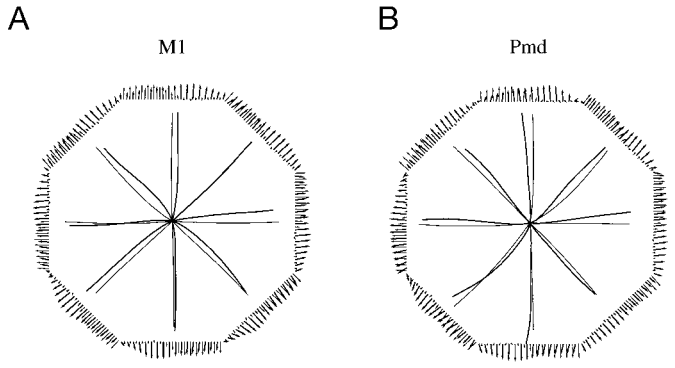


FIG. 14. Population vectors and trajectories. The outer octagonal figures contain vectorgrams of the velocity (thin) and population (thick) vectors for movements to each of the 8 targets of the center→out task. *A*: generated using 897 M1 cells. *B*: composed of 142 Pmd cells. Each set of vectors represents a time series (time advances in a counterclockwise direction) composed of 17 total vectors: 7 during the reaction period and 10 during the movement period. On average, the length of each vector corresponds to ~25 ms of time. The 10 population vectors that correlated best to the velocity vectors occurring over the movement period were integrated in time. The results of this integration can be seen in the center of each figure. The thin lines represent finger trajectory, whereas the thick lines represent the population trajectory.

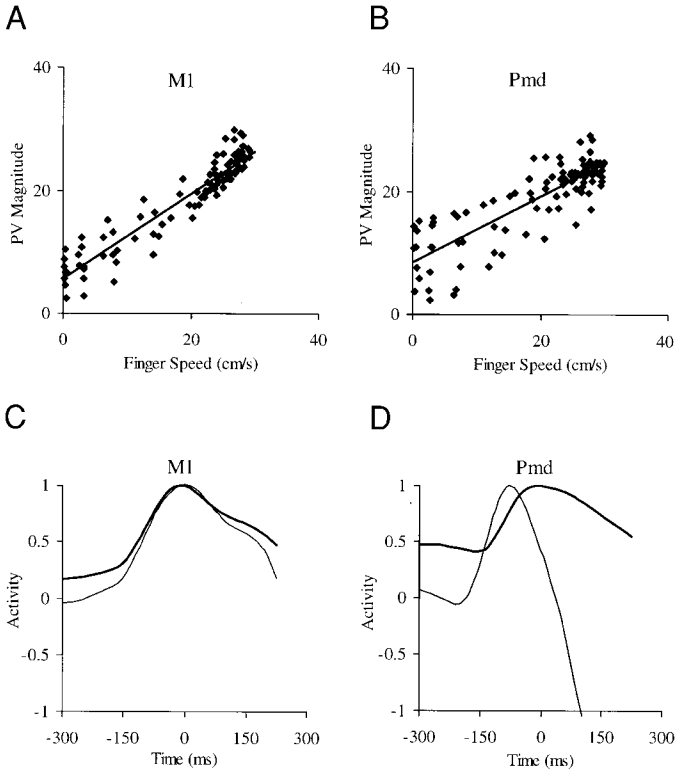


FIG. 15. *A*: regression between finger speed and population vector magnitudes of M1 cells. *B*: similar regression performed on premotor population vector magnitudes resulted in a lower correlation. *C*: comparison of average population vector magnitudes (thick lines) and ensemble nondirectional components (thin lines). The nondirectional and population magnitude profiles for M1 cells are very similar ($r^2 = 0.96$), and both represent well the average finger speed. *D*: Pmd cells generate very different results ($r^2 = 0.07$) when comparing population vector magnitude to nondirectional activity. *Time 0* represents movement onset.

clockwise direction. The movement vectors (thin lines) are short and point in random directions during the RT, whereas the population vectors (thick lines) generally are initially short but quickly elongate during the middle of RT before movement begins. Vector field correlations (Shadmehr and Mussa-Ivaldi 1994) between the movement and population vectors were performed at varying lags to find the highest correlation. The M1 population vectors had a maximum correlation of 0.97 at a lag of 145 ms, whereas the Pmd population vectors had a maximum correlation of 0.87 at a lag of 170 ms.

Neural trajectories can be formed by integrating the population vectors (multiplying by the average binwidth and adding them tip-to-tail). Using the lag information from the vector field correlations above, the 10 population vectors that temporally corresponded to the movement period were integrated into the trajectories shown in the center of Fig. 14*A*. The M1 neural trajectories match the hand trajectories. Figure 14*B* shows the population vectors and trajectories generated from the premotor cortical data. Like the M1 cells, the Pmd cells provide a good overall representation of the movement trajectory.

The population vector magnitudes were regressed to finger speed across all eight targets and for each of the 10 movement bins. Figure 15*A* shows the results of this regression for the M1 cells. A correlation coefficient of 0.94 was found at a lag of 145 ms. Figure 15*B* shows the regression results for the premotor data. In this case, a correlation coefficient of 0.83 was found at a lag of 166 ms, which is a shorter lag than the 190-ms lag found from cross-correlating the nondirectional component with finger speed (Fig. 5).

Averaging the magnitudes of the population vectors across all eight directions yields a population vector "velocity" profile that can be directly compared with the ensemble nondirectional profiles shown in Fig. 5. Based on M1 activity, both methods produce an accurate representation of the actual speed (Fig. 15*C*). Figure 15*D* shows the results of a similar procedure performed on the premotor activity. The two curves have very different temporal profiles. The Pmd nondirectional component peaks during the portion of the movement where the population magnitude is changing the most. This Pmd component is better correlated to acceleration, whereas the population vector magnitudes are well related to speed in this portion of the movement. The method used to generate population vectors removes additive factors that are common across all targets. Thus the nondirectional component ($b_n$), derived as a common effect across all targets, is not pertinent to the construction of population vectors. Consequently, the effect of speed on population vector length is due solely to the interaction between speed and direction ($b_x$ and $b_y$ terms; see APPENDIX).

## DISCUSSION

The directional sensitivity of motor cortical cells has been described primarily with a single estimated firing rate for each reach. To demonstrate a continuous relation between movement parameters and cortical activity, it is necessary to examine those components that vary in time. During reaching, the arm's trajectory is fairly straight; movement direction is approximately constant. In contrast, the speed of the arm varies with a bell-shaped velocity profile, making it useful to compare this parameter to firing rate over time. The design of this reaching paradigm with constant movement direction and time-varying speed allowed us to separate the effects of these two parameters on discharge rate. Our analysis revealed that speed acts both independently and interactively with direction to modulate discharge activity. This was the motivation for including both nondirectional ($b_n$) and directional ($b_x$, $b_y$) terms in *Eq. 1*.

The idea that speed and direction information is combined in the activity of single cells in the form of *Eq. 1* was addressed and supported with four different approaches. The directional cancellation procedure showed that single-cell activity could be separated into nondirectional and directional components. A regression between peak speed and firing rate in individual trials showed that there was an interaction between speed and discharge rate so that speed was acting as gain factor on the directional tuning curve. The validity of *Eq. 1* was tested directly with multiple regression. And, finally the magnitudes of the population vectors calculated during this task were shown to be directly proportional to speed in a way that depended on the form of *Eq. 1*.

Initially we removed the directional component of activity by adding movements in opposite directions. Because the directional responses of these cells are symmetrical (cosine tuned), the directional modulation is equal and opposite about some mean value. After removing the directional component, the residual (nondirectional) pattern was found to be highly

correlated with the speed profile. Speed also acts as a multiplier of the directional modulation in single cells after the nondirectional effect was subtracted from the discharge profile (Fig. 10). One way to visualize how discharge activity is affected by the combination of speed and direction is with the tuning functions in Fig. 11. Speed tends to modulate cortical discharge rate primarily when moving in the preferred direction, suggesting that *speed* acts as a gain factor of the directional tuning function. Previously, a gain factor was used to describe the receptive field of posterior parietal cells because the angle of the eyes in the head potentiated or attenuated the retinotopic tuning function (Andersen et al. 1985). This type of interaction differs from the effect static loads have on the directional tuning in motor cortical cells (Kalaska et al. 1989). Loads tended to shift the tuning function of these cells as an additive offset. This is similar to the effect of movement amplitude on the tuning functions of pallidal cells (Turner and Anderson 1997).

### *Continuous control of reaching*

Our results show that direction and speed are represented continuously in the discharge activity of single cells during reaching. Point-to-point movements have been considered classically as discrete events. Reaching movements consist of an initial ballistic transport component characterized by a stereotypic force pulse and velocity profile. The shape of the force pulse remains the same, but its magnitude is graded with different amplitudes of movement (Hollerbach and Flash 1982; Morasso 1981). During this phase of movement, the effect of sensory input may be delayed until the terminal phase of the reach as the hand approaches the target (Brooks 1974; Massey et al. 1986; Megaw 1974; Paillard 1982; Paillard and Brouchon 1974). The terminal phase of reaching is under visual control, and it is here that accuracy constraints come into play (Fitts and Peterson 1964; Meyer et al. 1982; Soechting 1984; Woodworth 1899). Because most of the distance covered during the reach is in the initial transport phase and this is unaffected by ongoing sensation or the absence of it (Bossom 1974; Taub et al. 1975), it was suggested that the control of this movement was completely specified before it began (Ghez and Vicario 1978; Kelso and Holt 1980).

The concept of open-loop control during reaching led to the idea that only the endpoint or target need be specified by the nervous system and that the springlike properties of the arm would ensure the proper delivery of the hand to the preset target location (Polit and Bizzi 1979). Although soon abandoned (Bizzi et al. 1982, 1984), this idea was replaced with similar theories using equilibrium points that shifted during the movement (Bizzi et al. 1984; Flash 1987; Hatsopoulos 1994; Won and Hogan 1995). The equilibrium trajectory hypothesis supposes that a time series of muscle tensions is calculated before movement initiation. Each combination of terms can be represented by a point in space where the arm would rest if those tensions were frozen at an instant in time.

In experiments where reaching was transiently perturbed with amplified Coriolis forces, subjects in the dark initially made unusually curved trajectories, missing the target (Lackner and Dizio 1994). Because Coriolis forces are absent at the end of the movement when the arm is stationary, the hand should, under the influence of the equilibrium trajectory, arrive at the correct target location. Furthermore, subjects rapidly modified their abnormally curved trajectories, making them straighter on subsequent trials. This shows that the subjects were compensating for the unusual inertial loads placed on the arm, an operation that would be unnecessary if the equilibrium trajectory was effective. This also shows that there was a continuous monitoring of afferent information during the movement that was used to compensate for the abnormal trajectory.

One aspect of the equilibrium-point hypothesis is that the equilibrium-point and actual trajectories should be similar. This will happen only if the limb is sufficiently stiff during the movement (Flash 1987). However, recent elegant measurements show the arm to be much less stiff in the middle of the trajectory than predicted (Gomi and Kawato 1996). The measured stiffness of the arm was used to construct equilibrium-point trajectories, and from these, velocity profiles were calculated. These calculated profiles were multipeaked and quite different from those of the actual trajectory.

These behavioral studies show that there is a continuous process underlying the generation of reaching. This process is characterized by a temporal template and is not immediately affected by sensory feedback. Our neuronal results show that implementation of this process is incremental throughout the task. Reaching is controlled by an ongoing process that keeps the hand moving continuously along a specified trajectory.

### *Neural recordings*

Neural activity in the motor cortex varies in a systematic way during reaching movements. The center→out paradigm was originally designed to test the responses of motor cortical cells to movement direction. Integrated activity within these approximately straight reaches is characterized with a cosine tuning function (Caminiti et al. 1990b; Georgopoulos et al. 1983, 1988). Time series of population vectors constructed during a three-dimensional version of this task closely matched a corresponding series of movement vectors (Georgopoulos et al. 1988). During drawing movements where both the direction and speed of the arm changes within the movement, the length and direction of the population and movement vectors matched (Schwartz 1993, 1994a). These results showed that motor cortical activity, when considered as an ensemble, did predict the arm's trajectory in a continuous manner.

Such a demonstration is more difficult using only the responses of individual cells. In this study we developed a model that explains how speed and direction can be encoded at the same time in the activity pattern of a single cell. In an earlier study, Ashe and Georgopoulos (1994) performed a multiple regression of target direction, hand position, velocity, and acceleration to discharge rate. This analysis showed that motor and parietal cortical cells had activity that was correlated with all of these parameters. Direction accounted for most of the variance in discharge followed by speed and position of the hand. A very small part of the discharge activity was related to acceleration. The mean best lag between motor cortical activity and the movement parameters was −90 ms (cortical activity before movement). For the parietal cells, the mean lag was +30 ms (cortical activity after movement). Another analysis using multiple regression (Fu et al. 1995) found that the static parameters of direction, target position, and movement ampli-

tude (respectively) were represented sequentially in single motor cortical cell activity patterns. Our analysis is similar to that of Ashe and Georgopoulos because of the use of time-varying parameters. *Equation 1* included one kinematic parameter (velocity) while the model of Ashe and Georgopoulos included three kinematic parameters (position, velocity, and acceleration) as well as a constant target parameter (target direction). The explanatory power of our model was generated by the use of both a direction-dependent (velocity) and a direction-independent speed term.

Combining the activity of all the cells (categorizing targets by preferred direction) and regressing to *Eq. 1* led to an "ensemble" or overall $r^2$ of 0.99. This result is much larger than any of the of individual cell regressions used to create the average activity. Several factors could be responsible for this ensemble superiority. The effect of movement parameters that influence the discharge of individual cells in an inconsistent manner will be removed by averaging across cells, whereas those parameters that many cells have in common will be more apparent. In the same way, stochastic noise in cortical firing rates would also be reduced and would lead to a higher fidelity signal. This is the fundamental meaning of the population vector.

The interaction of speed and direction as factors in the modulation of cortical activity can be an important consideration when studying reaching movements. For instance, in the center→out task, if the subject moves faster in some directions than others, the differences in speed will lead to an errant measurement of preferred direction. This may be a special problem when performing a task with different arm orientations (Caminiti et al. 1991; Scott and Kalaska 1995, 1997). Nonuniform movement speeds to different targets will appear to alter the preferred direction of the cell; however, it will not alter population vector direction, only its magnitude.

### *Premotor activity*

Activity patterns of single premotor cortical cells are similar to those of M1 cells in this task. The major difference between the two cell types is in their nondirectional components. The premotor nondirectional component peaks faster, and the overall width of this profile is narrower than the velocity profile. Consistent with other reports (Caminiti et al. 1991; Crammond and Kalaska 1996; Kurata and Tanji 1986), this suggests that the premotor contribution to reaching is earlier and more transient than M1. When aligned with the beginning of movement (15% maximum), the nondirectional activity corresponds better to the initial acceleration profile of the hand rather than velocity. The speed-direction interaction is expressed with greater sensitivity in these cells when compared with M1, with a regression slope between activity and speed that is twice as steep in the preferred direction but half as steep in the anti-preferred direction. The observation that these cells are speed and direction sensitive shows that the representation of these parameters does not arise de novo in the primary motor cortex. Direction, speed and amplitude sensitivity has been found in the cellular activity of many areas linked anatomically to M1 (Crutcher and Alexander 1990; Fortier et al. 1989; Ruiz et al. 1995; Schwartz 1994b; Turner and Anderson 1997).

### *EMG*

Using the center→out task we found our sample of proximal-arm EMG activity levels to be cosine-tuned in the planar movement task. This might be taken as support for the direct control of muscle activity by the motor cortex because both single cortical cells and muscle activity are directionally tuned. However, there are clear differences between the two types of activity in this task. Perhaps the most important distinction is that the preferred directions of the sampled muscles were all oriented vertically, whereas the distribution of motor cortical preferred directions were uniformly distributed. It is likely that the preferred directions of the muscles in this task are oriented to counteract gravity because this is an important torque component for a vertically orientated center→out task (Kakavand et al. 1996). Previous studies involving EMG activity in a horizontally oriented center→out task found that muscle preferred directions were evenly distributed (Georgopoulos et al. 1984). Because the movements in that study were in a near-horizontal plane and the monkey's arm was semi-supported by the manipulandum, gravity would be expected to have a negligible role on muscle dynamics.

Another interesting difference between the center→out results of Georgopoulos et al. (1984) and our results is the difference in preferred directions of some muscles. For instance, the latissiumus dorsi in the horizontal study had a preferred direction that pulled the hand backward while in the vertical task, the preferred direction was oriented superiorly and medially. Without joint angle information from both tasks, it is difficult to speculate; however, the primary functions of the latissiumus dorsi are shoulder extension, which would result in a posterior preferred direction, and adduction, which would yield a medial preferred direction. Thus both preferred directions are a probable result of agonist activity in the two different tasks. It is likely that arm orientation can affect the preferred direction of a muscle.

It is interesting that the nondirectional component of EMG activity is well correlated with the velocity profile in contrast to the expectation that agonist activity would look more like the initial phase of the acceleration profile as found in typical single-joint movements (Gottlieb et al. 1989). When multiple muscles are simultaneously active across the same joint in unconstrained arm movements, the combination of activity, perhaps asynchronous, across the other muscles as well as the nonmuscle derived forces acting on the limb complicate the relation between the forces produced in individual muscles and the actual torques generated across a joint (Bernstein 1967; Flanders et al. 1994; Gottlieb 1996).

Another interesting feature is the relationship between speed and EMG activity during movements in different directions. As expected, EMG activity increases when moving faster in a muscle's preferred direction. This positive correlation with speed disappears or becomes negative when moving in other directions. Antagonistic bursts are often present if a movement is made fast enough; however, with our well-trained subjects moving at peak speeds $<40$ cm/s, antagonist bursts were not evident. The data in this study suggest that the way a muscle contributes to changes in movement speed in a particular direction differs from that of M1 cells, which showed positive correlation with speed throughout all directions.

*Population activity*

The representation of trajectory-related information present in the population of recorded activity is easy to visualize using a simple algorithm. Summing the activity patterns of many cells together vectorially results in a time series of population vectors that represents the instantaneous velocity of the finger as it moves to the target in the center→out task. Our knowledge of the way direction and speed are encoded by single cells can help explain why the population vector, when integrated, is such a robust predictor of the finger's trajectory. To construct a population vector of appreciable length, there must be some asymmetry in the vector components used to derive it. Because the distribution of preferred directions in the population is uniform, the asymmetry stems from the uneven distribution of individual firing rates at the instant when the population vector is calculated. We have shown that both direction and speed will contribute to the uneven distribution of firing intensities across the population. Cells with preferred directions near the movement direction will fire faster, and these larger contributions will make the population vector point in the direction of movement. If all the cells in the population now increased their discharge rate by the same amount (e.g., adding 10 spikes/s to all cells), the resulting population vector would point in the same direction and have the same magnitude. This is a consequence of the normalization used in *Eq. 4*. In fact, any factor that changed the activity of all cells in the population by an additive constant would not change the magnitude or orientation of the population vector (see APPENDIX). Interestingly, if the effect of this additive factor is not constant in all directions when performing the center→out task, the preferred direction will appear to change when the experimental parameters are varied (e.g., presence or absence of external loads). Changes in preferred direction of individual cells without changes in the population vector direction has been reported in several studies (Caminiti et al. 1990a,b; Chen and Wise 1996; Scott and Kalaska 1995). However, an increase or decrease in the firing rate of all cells by the same *ratio*, as our results show (Fig. 11), will change the length of the population vector by that ratio (see APPENDIX). This is the basis for the robust relation between the population vector magnitude and speed. Speed acts as a gain factor on the firing rates of individual cells, increasing the amplitude of the tuning function. As a result, the speed effect is emphasized in those cells firing fastest (i.e., those with preferred directions near the movement direction), and they will have an increased contribution to the population vector. This illustrates how the multiple representation of parameters in the activity patterns of single cells can be easily extracted using a population algorithm.

## APPENDIX

Here we derive the relation between time-varying parameters that influence single-cell discharge rate and population vector magnitude. The theoretical length of a population vector can be calculated by combining the motor cortical cell model of *Eq. 3* and the population vector algorithm of *Eq. 4*. The formula for a population vector using the average discharge rates from a population of cells collected over a movement to *target 1* is

$$\overline{PV}_1 = \sum_{i=1}^{\text{num cells}} \frac{\bar{D}_{i,1} - B_{0,i}}{\bar{D}_{i,\max}} \cdot \frac{B_{x,i}}{\bar{D}_{i,\max}} \tag{A1}$$

*Equation* A*1* is for movements along the positive *x*-axis; thus there is no *y* component and $P\bar{V}_1$ is equal to the magnitude of the population vector. $\bar{D}_{i,1}$ corresponds to the average firing rate of cell *i* to *target 1* and $\bar{D}_{i,\max}$ corresponds to the maximum depth of modulation for cell *i* across all targets. Movements in this direction correspond to a direction of zero degrees; therefore the average discharge of cell *i* during movements to *target 1* can be written as

$$\bar{D}_{i,1} = B_{0,i} + \bar{D}_{i,\max} \cos(\theta_{pd}) \tag{A2}$$

Likewise, the *x* component of cell *i*'s preferred direction can be written as

$$\frac{B_{x,i}}{\bar{D}_{i,\max}} = \cos(\theta_{pd}) \tag{A3}$$

Substituting *Eqs.* A*2* and A*3* into *Eq.* A*1* yields

$$\overline{PV}_1 = \sum_{i=1}^{\text{num cells}} \cos^2(\theta_{pd}) \tag{A4}$$

Assuming a uniform directional distribution of *N* cells, *Eq.* A*4* can be rewritten as

$$\overline{PV}_1 = \frac{N}{2\pi} \int_0^{2\pi} \cos^2(\theta) d\theta \tag{A5}$$

Solving:

$$\overline{PV}_1 = \frac{N}{2\pi} \left[ \frac{\theta}{2} + \frac{\sin(2\theta)}{4} \right] \Bigg|_0^{2\pi} = \frac{N}{2} \tag{A6}$$

Thus for a population of cells with a uniform distribution of preferred directions with discharge rates described completely by cosine tuning, the lengths of the population vectors for a center→out task would be equal to one-half the number of cells in the population.

We have shown that population vector length is directly proportional to finger speed; therefore calculating theoretical population vector lengths for both a fast and slow movement should result in different values. Now assuming speed affects discharge rate in the manner proposed in *Eq. 1*, a ratio of population vector lengths in the slow versus fast task can be calculated. Two forms of *Eq.* A*2* would be generated: one for the fast trials and one for the slow trials. However, *Eq.* A*3* would be unchanged. Recalculating population vector magnitudes for both populations yields

$$\overline{PV}_{1,HS} = \sum_{i=1}^{\text{num cells}} \frac{\bar{D}_{i,\max,HS} \cos^2(\theta_{pd}) + (B_{0,i,HS} - B_{0,i}) \cos(\theta_{pd})}{\bar{D}_{i,\max,HS}} \tag{A7}$$

$$\overline{PV}_{1,LS} = \sum_{i=1}^{\text{num cells}} \frac{\bar{D}_{i,\max,LS} \cos^2(\theta_{pd}) + (B_{0,i,LS} - B_{0,i}) \cos(\theta_{pd})}{\bar{D}_{i,\max,HS}} \tag{A8}$$

where the subscripts *HS* and *LS* correspond to the high-speed and low-speed trials, respectively. (Both equations are normalized by the high-speed maximum discharge rate because it would be the larger overall firing rate.) Converting to integrals and solving yields

$$\overline{PV}_{1,HS} = \frac{N}{2} \tag{A9}$$

$$\overline{PV}_{1,LS} = \frac{N}{2} \frac{\bar{D}_{\max,LS}}{\bar{D}_{\max,HS}} \tag{A10}$$

The lengths of the population vectors are dependent only on the ratios of the depths of modulation of the cells for the two different trials. Although the $B_0$ term could vary with speed, it would have no effect on the population vector lengths. The proof above was based on

average population vectors (*Eq. 3*); however, the results would be the same for a multi-bin analysis. Thus the terms $b_0$ and $b_n$ as defined in *Eq. 1* would similarly have no effect on population vector length.

A. Kakavand trained the animals and assisted in the experiments, J. Adams provided support in EMG data collection, and E. Lumer provided mathematical assistance.

This work was supported by the Neurosciences Research Foundation, the Barrow Neurological Institute, and National Institute of Neurological Disorders and Stroke Grant NS-26375.

Address for repint requests: A. B. Schwartz, The Neurosciences Institute, 10640 John Jay Hopkins Dr., San Diego, CA 92121.

Received 22 July 1996; accepted in final form 28 November 1997.

## REFERENCES

ALEXANDER, G. E. AND CRUTCHER, M. D. Preparation for movement: neural representations of intended direction in three motor areas of monkey. *J. Neurophysiol.* 64: 133–150, 1990a.

ALEXANDER, G. E. AND CRUTCHER, M. E. Neural representations of the target (goal) of visually guided arm movements in three motor areas of the monkey. *J. Neurophysiol.* 65: 164–178, 1990b.

ANDERSEN, R. A., ESSICK, G. K., AND SIEGEL, R. M. The encoding of spatial location by posterior parietal neurons. *Science* 230: 456–458, 1985.

ASANUMA, H. AND ROSEN, I. Topographical organization of cortical efferent zones projecting to distal forelimb muscles in the monkey. *Exp. Brain Res.* 14: 243–256, 1972.

ASHE, J. AND GEORGOPOULOS, A. P. Movement parameters and neural activity in motor cortex and area 5. *Cereb. Cortex* 6: 590–600, 1994.

BATSCHELET, E. *Circular Statistics in Biology.* London: Academic, 1981.

BAUSWEIN, E., FROMM, C., WERNER, W., AND ZIEMANN, U. Phasic and tonic responses of premotor and primary motor cortex neurons to torque changes. *Exp. Brain Res.* 86: 303–310, 1991.

BERNSTEIN, N. A. *The Coordination and Regulation of Movements.* Oxford, UK: Pergamon, 1967.

BIZZI, E., ACCORNERO, N., CHAPPLE, W., AND HOGAN, N. Arm trajectory formation in monkeys. *Exp. Brain Res.* 46: 139–143, 1982.

BIZZI, E., ACCORNERO, N., CHAPPLE, W., AND HOGAN, N. Posture control and trajectory formation during arm movement. *J. Neurosci.* 4: 2738–2744, 1984.

BOSSOM, J. Moving without proprioception. *Brain Res.* 71: 285–296, 1974.

BROOKS, V. B. Some examples of programmed limb movements. *Brain Res.* 71: 299–308, 1974.

BURBAUD, P., DOEGLE, C., GROSS, C., AND BIOULAC, B. A quantitative study of neuronal discharge in areas 5, 2, and 4 of the monkey during fast arm movements. *J. Neurophysiol.* 66: 429–443, 1991.

BUTLER, E. G., HORNE, M. K., AND CHURCHWARD, P. R. A frequency analysis of neuronal activity in monkey thalamus, motor cortex and electromyograms in wrist oscillations. *J. Physiol. (Lond.)* 445: 49–68, 1992.

CAMINITI, R., JOHNSON, P. B., BURNOD, Y., GALLI, C., AND FERRAINA, S. Shift of preferred directions of premotor cortical cells with arm movements performed across the workspace. *Exp. Brain Res.* 83: 228–232, 1990a.

CAMINITI, R., JOHNSON, P. B., GALLI, C., FERRAINA, S., AND BURNOD, Y. Making arm movements within different parts of space: the premotor and motor cortical representation of a coordinate system for reaching to visual targets. *J. Neurosci.* 11: 1182–1197, 1991.

CAMINITI, R., JOHNSON, P. B., AND URBANO, A. Making arm movements within different parts of space: Dynamic aspects in the primate motor cortex. *J. Neurosci.* 10: 2039–2058, 1990b.

CHEN, L. L. AND WISE, S. P. Evolution of directional preferences in the supplementary eye field during acquisition of conditional oculomotor associations. *J. Neurosci.* 16: 3067–3081, 1996.

CRAMMOND, D. J. AND KALASKA, J. F. Differential relation of discharge in primary motor cortex and premotor cortex to movements versus actively maintained postures during a reaching task. *Exp. Brain Res.* 108: 45–61, 1996.

CRUTCHER, M. D. AND ALEXANDER, G. E. Movement-related neuronal activity selectively coding either direction or muscle pattern in three motor areas of the monkey. *J. Neurophysiol.* 64: 151–163, 1990.

DETTMERS, C., LEMON, R. N., STEPHAN, K. M., FINK, G. R., AND FRACKOWIACK, R. S. Cerebral activation during the exertion of sustained force in man. *Neuroreport* 7: 2103–2110, 1996.

EVARTS, E. V. Relation of pyramidal tract activity to force exerted during voluntary movement. *J. Neurophysiol.* 31: 14–27, 1968.

FETZ, E. E. AND CHENEY, P. D. Muscle fields of primate corticomotoneuronal cells. *J. Physiol. Paris* 74: 239–245, 1978.

FETZ, E. E. AND FINNOCHIO, D. V. Correlations between activity of motor cortex cells and arm muscles during operantly conditioned response patterns. *Exp. Brain Res.* 23: 217–240, 1975.

FITTS, P. M. AND PETERSON, J. R. Information capacity of discrete motor responses. *J. Exp. Psychol.* 67: 103–112, 1964.

FLAMENT, D. AND HORE, J. Relations of motor cortex neural discharge to kinematics of passive and active elbow movements in the monkey. *J. Neurophysiol.* 60: 1268–1284, 1988.

FLANDERS, M., PELLEGRINI, J. J., AND SOECHTING, J. F. Spatial/temporal characteristics of a motor pattern for reaching. *J. Neurophysiol.* 71: 811–813, 1994.

FLASH, T. The control of hand equilibrium trajectories in multi-joint arm movements. *Biol. Cybern.* 57: 257–274, 1987.

FORTIER, P. A., KALASKA, J. F., AND SMITH, A. M. Cerebellar neuronal activity related to whole-arm reaching movements in the monkey. *J. Neurophysiol.* 62: 198–211, 1989.

FRITSCH, G. AND HITZIG, E. Ueber dir elektrische Erregbarkeit des Grosshirns. *Arch. Anat. Physiol. Lpz.* 37: 300–332, 1870.

FU, Q.-G., FLAMENT, D., COLTZ, J. D., AND EBNER, T. J. Temporal encoding of movement kinematics in the discharge of primate primary motor and premotor neurons. *J. Neurophysiol.* 73: 836–854, 1995.

FU, Q. J., SUAREZ, J. I., AND EBNER, T. J. Neuronal specification of direction and distance during reaching movements in the superior precentral premotor area and primary motor cortex of monkeys. *J. Neurophysiol.* 70: 2097–2116, 1993.

GEORGOPOULOS, A. P., ASHE, J., SMYRNIS, N., AND TAIRA, M. The motor cortex and the coding of force. *Science* 256: 1692–1695, 1992.

GEORGOPOULOS, A. P., CAMINITI, R., KALASKA, J. F., AND MASSEY, J. T. Spatial coding of movement: a hypothesis concerning the coding of movement direction by motor cortical populations. *Exp. Brain Res. Suppl.* 7: 327–336, 1983.

GEORGOPOULOS, A. P., KALASKA, J. F., CAMINITI, R., AND MASSEY, J. T. On the relations between the direction of two-dimensional arm movements and cell discharge in primate motor cortex. *J. Neurosci.* 2: 1527–1537, 1982.

GEORGOPOULOS, A. P., KALASKA, J. F., CRUTCHER, M. D., CAMINITI, R., AND MASSEY, J. T. The representation of movement direction in the motor cortex: single cell and population studies. In: *Dynamic Aspects of Neocortical Function*, edited by G. E. Edelman, W. E. Gall, and W. M. Cowan. New York: Wiley, 1984, p. 501–524.

GEORGOPOULOS, A. P., KALASKA, J. F., AND MASSEY, J. T. Spatial trajectories and reaction times of aimed movements: Effects of practice, uncertainty and change in target location. *J. Neurophysiol.* 46: 725–743, 1981.

GEORGOPOULOS, A. P., KETTNER, R. E., AND SCHWARTZ, A. B. Primate motor cortex and free arm movements to visual targets in three-dimensional space. II. Coding of the direction of movement by a neuronal population. *J. Neurosci.* 8: 2928–2937, 1988.

GHEZ, C. AND VICARIO, D. The control of rapid limb movement in the cat. II. Scaling of isometric force adjustments. *Exp. Brain Res.* 33: 191–202, 1978.

GOMI, H. AND KAWATO, M. Equilibrium-point control hypothesis examined by measured arm stiffness during multijoint movement. *Science* 272: 117–120, 1996.

GOTTLIEB, G. L. On the voluntary movement of compliant (inertial-viscoelastic) loads by parcellated control mechanisms. *J. Neurophysiol.* 76: 3207–3229, 1996.

GOTTLIEB, G. L. AND AGARWAL, G. C. Filtering of electromyographic signals. *Am. J. Phys. Med.* 49: 142–146, 1970.

GOTTLIEB, G. L., CORCOS, D. M., AND AGARWAL, G. C. Strategies for the control of voluntary movements with one mechanical degree of freedom. *Behav. Brain Sci.* 12: 189–250, 1989.

GRAY'S ANATOMY. 36th British Edition. Edinburgh: Churchill Livingstone, 1980.

HAMADA, I. Correlation of monkey pyramidal tract neuron activity to movement velocity in rapid wrist flexion movement. *Brain Res.* 230: 384–389, 1981.

HATSOPOULOS, N. G. Is a virtual trajectory necessary in reaching movements? *Biol. Cybern.* 70: 541–551, 1994.

HOLLERBACH, J. M. AND FLASH, T. Dynamic interactions between limb segments during planar arm movement. *Biol. Cybern.* 44: 67–77, 1982.

HUMPHREY, D. R., SCHMIDT, E. M., AND THOMPSON, L.V.D. Predicting measures of motor performance from multiple cortical spike trains. *Science* 179: 758–762, 1970.

JACKSON, J. H. Cases of partial convulsion from organic brain disease, bearing on the experiments of Hitzig and Ferrier. *Medical Times Gazette* 1: 578–579, 1875.

KAKAVAND, A., MORAN, D., AND SCHWARTZ, A. B. Dynamic correlations of motor cortical activity with kinetic and kinematic parameters of hand movement. *Soc. Neurosci. Abstr.* 22: 1830, 1996.

KALASKA, J. F., COHEN, D.A.D., HYDE, M. L., AND PRUD'HOMME, M. A comparison of movement direction-related versus load direction-related activity in primate motor cortex, using a two-dimensional reaching task. *J. Neurosci.* 9: 2080–2102, 1989.

KALASKA, J. F. AND CRAMMOND, D. J. Cerebral control mechanisms of reaching movements. *Science* 255: 1517–1523, 1992.

KELSO, J.A.S. AND HOLT, K. G. Exploring a vibratory system analysis of human movement production. *J. Neurophysiol.* 43: 1183–1196, 1980.

KURATA, K. AND TANJI, J. Premotor cortex neurons in macaques: activity before distal and proximal forelimb movements. *J. Neurosci.* 6: 403–411, 1986.

LACKNER, J. R. AND DIZIO, P. Rapid adaptation to Coriolis-force perturbations of arm trajectory. *J. Neurophysiol.* 72: 299–313, 1994.

LANDGREN, S., PHILLIPS, C. G., AND PORTER, R. Cortical fields of origin of the monosynaptic pyramidal pathways to some alpha motoneurones of the baboon's hand and forearm. *J. Physiol. (Lond.)* 161: 112–125, 1962.

LEMON, R. N., MUIR, R. B., AND MANTEL, G.W.H. The effects upon the activity of hand and forearm muscles of intracortical stimulation in the vicinity of corticomotor neurons in the conscious monkey. *Exp. Brain Res.* 66: 621–637, 1987.

LEYTON, A.S.F. AND SHERRINGTON, C. S. Observations and the excitable cortex of the chimpanzee, orang-utan and gorilla. *Q. J. Exp. Physiol.* 11: 135–222, 1917.

LOEB, G. E. AND GANS, C. *Electromyography for Experimentalists.* Chicago, IL: Univ. of Chicago Press, 1986.

LUCIER, G. E., RUEGG, D. C., AND WIESENDANGER, M. Responses of neurones in motor cortex and in area 3A to controlled stretches of forelimb muscles in cebus monkeys. *J. Physiol. (Lond.)* 251: 833–853, 1975.

MAIER, M. A., BENNETT, K.M.B., HEPP-REYMOND, M.-C., AND LEMON, R. N. Contribution of the monkey corticomotoneuronal system to the control of force in precision grip. *J. Neurophysiol.* 69: 772–785, 1993.

MANTEL, G. W. AND LEMON, R. N. Cross-correlation reveals facilitation of single motor units in thenar muscles by single corticospinal neurones in the conscious monkey. *Neurosci. Lett.* 77: 113–118, 1987.

MASSEY, J. T., SCHWARTZ, A. B., AND GEORGOPOULOS, A. P. On information processing and performing a movement sequence. In: *Generation and Modulation of Action Patterns*, edited by C. Fromm and H. Heuer. *Exp. Brain Res. Series 15*, 1986, p. 242–251.

MEGAW, E. D. Possible modification to a rapid on-going programmed manual response. *Brain Res.* 71: 425–441, 1974.

MEYER, D. E., SMITH, J.E.K., AND WRIGHT, C. E. Models for the speed and accuracy of armed movements. *Psychol. Rev.* 89: 449–482, 1982.

MORASSO, P. Spatial control of arm movements. *Exp. Brain Res.* 42: 223–227, 1981.

MOUNTCASTLE, V. B., LYNCH, J. C., GEORGOPOULOS, A., SAKATA, H., AND ACUNA, C. Posterior parietal association cortex of the monkey: command functions for operations within extrapersonal space. *J. Neurophysiol.* 38: 871–908, 1975.

MOUNTCASTLE, V. B., TALBOT, W. H., SAKATA, H., AND HYVARINEN, J. Cortical neuronal mechanisms in the flutter vibration studied in unanesthetized monkeys. Neuronal periodicity and frequency discrimination. *J. Neurophysiol.* 32: 452–484, 1969.

PAILLARD, J. The contribution of peripheral and central vision to visually guided reaching. In: *Analysis of Visual Behavior*, edited by D. J. Ingle, M. A. Goodale, and R.J.W. Mansfield. Cambridge, MA: MIT Press, 1982, p. 367–385.

PAILLARD, J. AND BROUCHON, M. A proprioceptive contribution to the spatial encoding of position cues for ballistic movements. *Brain Res.* 71: 273–284, 1974.

POLIT, A. AND BIZZI, E. Characteristics of the motor programs underlying arm movements in monkeys. *J. Neurophysiol.* 42: 183–192, 1979.

RICHMOND, B. J., OPTICAN, L. M., PODELL, M., AND SPITZER, H. Temporal encoding of two-dimensional patterns by single units in primate inferior temporal cortex. I. Response characteristics. *J. Neurophysiol.* 57: 132–146, 1987.

RUIZ, S., CRESPO, P., AND ROMO, R. Representation of moving tactile stimuli in the somatic sensory cortex of awake monkeys. *J. Neurophysiol.* 73: 525–537, 1995.

SANES, J. N., SUNER, S., AND DONOGHUE, J. P. Dynamic organization of primary motor cortical output to target muscles in adult rats. I. Long-term patterns of reorganization following motor or mixed peripheral nerve lesions. *Exp. Brain Res.* 79: 479–491, 1990.

SANES, J. N., WANG, J., AND DONOGHUE, J. P. Immediate and delayed changes of rat motor cortical output with new forelimb configurations. *Cereb. Cortex* 2: 141–152, 1992.

SCHAFER, E. A. The cerebral cortex. In: *Textbook of Physiology*, edited by E. A. Schafer. London: Young J. Pentland, 1900, p. 697–782.

SCHMIDT, E. M., JOST, R. G., AND DAVID, K. K. Re-examination of force relationship of cortical cell discharge patterns with conditioned wrist movements. *Brain Res.* 83: 213–223, 1975.

SCHWARTZ, A. B. Motor cortical activity during drawing movements. Single-unit activity during sinusoid tracing. *J. Neurophysiol.* 68: 528–541, 1992.

SCHWARTZ, A. B. Motor cortical activity during drawing movements: population response during sinusoid tracing. *J. Neurophysiol.* 70: 28–36, 1993.

SCHWARTZ, A. B. Direct cortical representation of drawing. *Science* 265: 540–542, 1994a.

SCHWARTZ, A. B. Distributed processing in cerebral cortex. *Cur. Opin. Neurobiol.* 4: 840–846, 1994b.

SCHWARTZ, A. B., KETTNER, R. E., AND GEORGOPOULOS, A. P. Primate motor cortex and free arm movements to visual targets in three-dimensional space. I. Relations between single cell discharge and direction of movement. *J. Neurosci.* 8: 2913–2927, 1988.

SCOTT, S. H. AND KALASKA, J. F. Changes in motor cortex activity during reaching movements with similar hand paths but different postures. *J. Neurophysiol.* 73: 2563–2567, 1995.

SCOTT, S. H. AND KALASKA, J. F. Reaching movements with similar had paths but different arm orientations. I. Activity of individual cells in motor cortex. *J. Neurophysiol.* 77: 826–852, 1997.

SHADMEHR, R. AND MUSSA-IVALDI, F. A. Adaptive representation of dynamics during learning of a motor task. *J. Neurosci.* 14: 3208–3224, 1994.

SOECHTING, J. F. Effective target size on spatial and temporal characteristics of a pointing movement in man. *Exp. Brain Res.* 54: 121–132, 1984.

SOKAL, R. R. AND ROHLF, F. J. *Biometry* (3rd ed.). New York: Freeman, 1995.

TAUB, E., GOLDBERG, I. A., AND TAUB, P. Deafferentation in monkeys pointing at a target without visual feedback. *Exp. Neurol.* 46: 178–186, 1975.

THACH, W. T. Correlation of neural discharge with pattern and force of muscular activity, point position, and direction of intended next movement in motor cortex and cerebellum. *J. Neurophysiol.* 41: 654–676, 1978.

TURNER, R. S. AND ANDERSON, M. E. Pallidal discharge related to the kinematics of reaching movements in two dimensions. *J. Neurophysiol.* 77: 1051–1074, 1997.

WOLTRING, H. J. A FORTRAN package for generalized, cross-validatory spline smoothing and differentiation. *Adv. Eng. Software* 8: 104–113, 1986.

WON, J. AND HOGAN, N. Stability properties of human reaching movement. *Exp. Brain Res.* 107: 125–136, 1995.

WOODWORTH, R. S. The accuracy of voluntary movement. *Psychol. Rev. Monogr. Suppl.* (whole 13) 3: 3: 1899.

WOOLSEY, C. N. Organization of somatic sensory and motor areas of the cerebral cortex. In: *Biological and Biochemical Bases of Behavior*, edited by H. F. Harlow and C. N. Woolsey. Madison, WI: Univ. of Wisconsin Press, 1958, p. 63–81.